HASBI, S., AMBER, I., HOSSAIN, M. and SAHARUDIN, M.S. 2025. Performance optimisation of solid oxide electrolyser cell (SOEC) using response surface method (RSM) for thermal gradient reduction. *International journal of sustainable energy* [online], 44(1), article number 2482837. Available from: https://doi.org/10.1080/14786451.2025.2482837

Performance optimisation of solid oxide electrolyser cell (SOEC) using response surface method (RSM) for thermal gradient reduction.

HASBI, S., AMBER, I., HOSSAIN, M. and SAHARUDIN, M.S.

2025

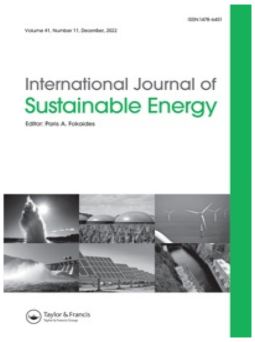

International Journal of Sustainable Energy

ISSN: (Print) (Online) Journal homepage: www.tandfonline.com/journals/gsol20

Performance optimisation of solid oxide electrolyser cell (SOEC) using response surface method (RSM) for thermal gradient reduction

Syafawati Hasbi, Ityona Amber, Mamdud Hossain & Mohd Shahneel Saharudin

To cite this article: Syafawati Hasbi, Ityona Amber, Mamdud Hossain & Mohd Shahneel Saharudin (2025) Performance optimisation of solid oxide electrolyser cell (SOEC) using response surface method (RSM) for thermal gradient reduction, International Journal of Sustainable Energy, 44:1, 2482837, DOI: 10.1080/14786451.2025.2482837

To link to this article: https://doi.org/10.1080/14786451.2025.2482837

INTERNATIONAL JOURNAL OF SUSTAINABLE ENERGY
2025, VOL. 44, NO. 1, 2482837
https://doi.org/10.1080/14786451.2025.2482837

Taylor & Francis
Taylor & Francis Group

Performance optimisation of solid oxide electrolyser cell (SOEC) using response surface method (RSM) for thermal gradient reduction

Syafawati Hasbi[a,b], Ityona Amber[a], Mamdud Hossain[a] and Mohd Shahneel Saharudin[a]

[a]School of Computing and Engineering Technology, Robert Gordon University, Aberdeen, UK; [b]Department of Mechanical Engineering, Faculty of Engineering, National Defence University Malaysia, Kuala Lumpur, Malaysia

ABSTRACT
The Solid Oxide Electrolyser Cell (SOEC) offers high-efficiency hydrogen production due to favourable thermodynamics and reaction kinetics at elevated temperatures. However, high operating temperatures increase energy consumption and thermal gradients, leading to material degradation and reduced durability. This study optimises SOEC operating conditions to minimise thermal gradients and enhance performance using numerical simulations and Response Surface Methodology (RSM). Key parameters examined include voltage (1.1–1.5 V), temperature (1073–1273 K), steam mass fraction (0.3–0.9), flow configurations, porosity, and charge transfer coefficients. Results show increasing voltage from 1.1 to 1.5 V raised current density from 0.75 A/cm^2 to 2.5 A/cm^2, while thermal gradients increased up to 15 K at higher temperatures. Counterflow configurations caused mid-cell hotspots, whereas parallel flow produced thermal gradient near the outlet. RSM optimisation identified optimal conditions of 1073, 1.5 V, and 0.9 steam mass fraction, reducing hotspot temperatures to 1086 K with minimal deviation. These findings support improved SOEC thermal management and hydrogen production efficiency.

ARTICLE HISTORY
Received 27 November 2024
Accepted 13 March 2025

KEYWORDS
Solid oxide electrolyser cell; response surface methods; green hydrogen production; computational fluid dynamics; thermal gradient optimisation

Nomenclature

α	axial point
C_i	mass fraction
c_p	specific heat
$D_{i,eff}$	effective diffusion coefficient of ith species
ε	porosity.
F	Faraday's constant
ΔG_f^o	Gibbs free energy.
ΔH_f	heat enthalpy.
I	total current
J	current density.
K	permeability.
k^{eff}	effective heat conductivity coefficient.
μ	dynamic viscosity (Pa.s)
n	numbers of electrons involved per reaction for the electrolytic reaction.
$\eta_{act,a}$	anode activation potential.

CONTACT Syafawati Hasbi s.hasbi1@rgu.ac.uk

$\eta_{act,c}$	cathode activation potential
$\eta_{con,a}$	anode concentration potential.
$\eta_{con,c}$	cathode concentration potential.
η_e	electrolysis efficiency
η_{ohm}	ohmic overpotential.
σ	electronic/ionic conductivity.
σ^{eff}	effectiveness of O^{2-} diffusion rate
φ_{mem}	ion potential.
n	number of variables.
n_c	number of centre point.
N	total number of design point.
σ_{sol}	conductivity of current collector.
P_{cell}	power produced by cell
Q	reaction coefficient.
R	ideal gas constant.
R_{cell}	overall effective resistance of cell.
R_{e}	resistance of electrode.
R_{el}	resistance of electrolyte.
R_{s}	resistance of separator.
S	surface area of the cell.
S_{mass}	source term for mas equation.
S_{mom}	source term for momentum equation
T	temperature.
$\vec{v}$	velocity vector.
V_{cell}	cell voltage
V_{Nernst}	Nernst voltage.
V_{ocv}	open cell voltage.
V_{rev}	reversible voltage
V_{tn}	thermal neutral voltage.

Abbreviations

AEC	Alkaline Electrolysis Cells.
BBD	Box Behnken Design.
CCD	Central Composite Design.
LSM	Lanthanum strontium manganite.
NiO	Nickel Oxide.
PEMEC	Proton Exchange Membrane Electrolysis Cells.
RSM	Response Surface Method.
SMF	Steam Mass Fraction.
SOEC	Solid Oxide Electrolyser Cell.
TPB	Triple Phase Boundary.
YSZ	Yttria-stabilized zirconia.

1. Introduction

Green hydrogen has become a key component in the shift toward sustainable energy systems, offering a clean alternative to fossil fuels and playing a significant role in decarbonising sectors such as transportation, industry, and power generation. Solid Oxide Electrolyser Cells (SOECs) are highly efficient technologies for hydrogen production, operating at elevated temperatures that enhance thermodynamic efficiency and enable direct steam electrolysis. This results in higher hydrogen production rates compared to conventional electrolyser technologies, such as Alkaline Electrolysis Cells (AEC) and Proton Exchange Membrane Electrolysis Cells (PEMEC). SOECs are particularly well-suited for integration with renewable energy sources, like solar and wind, as they can efficiently produce hydrogen even with fluctuating energy supplies. Water electrolysis, a more environmentally friendly and carbon-neutral method for hydrogen production, outperforms steam methane reforming, which, despite its efficiency, results in significant greenhouse gas emissions. While

PEMECs and AECs operate at lower temperatures (353–493 K), SOECs achieve higher conversion efficiencies at temperatures above 873 K, thanks to reduced Gibbs free energy and increased reaction rates, leading to higher efficiency and lower external energy requirements (Xu et al. 2023). The UK government aims to reduce carbon emissions by 78% compared to 1990 levels and to source 20–30% of its energy consumption from hydrogen by 2050, making SOECs a key technology in achieving these targets ("UK Hydrogen Strategy" 2021).

However, high operating temperatures present significant challenges in terms of material stability due to thermomechanical stresses and thermal degradation. Thermomechanical stress induced by temperature fluctuations within the cell increases the current density fluctuation, the thermal mismatch between cell components, the rate of degradation, and the probability of leaking, potentially leading to stack failure (Menon, Janardhanan, and Deutschmann 2014). SOECs typically operate at a higher current density than other electrolysers, leading to greater heat concentration within the cell and a subsequent rise in both the size and capital costs of the electrolyser (Kim, Park, and Lee 2013). In real-life applications, the variations in power during operation induce thermal stress. Petipas, Brisse, and Bouallou (2017) suggested that operating the cell below 60% of maximum power leads to a 10 K/cm thermal gradient in the cell which subsequently leads to stack failure. To mitigate these issues and enhance the longevity of the cell Aguiar, Adjiman, and Brandon (2023) recommend maintaining a temperature gradient of less than 10 K/cm during operation.

Two key parameters that highly affect the thermal performance of the cell are the operating voltage and temperature of the cell (Faghri and Guo 2005). The theoretical efficiency of a SOEC is close to 100% when operating at a thermoneutral voltage (1.29 V) (UK 2021) as depicted in Figure 1. Heat is either released or absorbed from surroundings when the cell operates below or above this voltage to offset the change in enthalpy and free energy (Fu et al. 2021). The maximum theoretical voltage of a cell is dependent on its operating temperature. Higher temperatures necessitate a lower theoretical voltage, enhance waste heat utilisation, and improve efficiency by intensifying the electrochemical reaction within the cell (Sofiah et al. 2024). However, thermal stress increases linearly with operating voltage due to an increase in temperature inside the cell which creates high local thermal stress (Cui et al. 2023) by the internal resistance of the cell, which reduces the electrolyser efficiency (Zheng et al. 2015). The temperature inside the cell fluctuates during its operation and it is highly beneficial to operate SOEC at a constant or near-thermoneutral voltage since isothermal operation ensures high efficiency, optimises cost, and simplifies the thermal management of the cell.

At present, experimental (Reytier et al. 2015; Schefold and Pöpke 2022; Zhang et al. 2015; Zheng et al. 2015) and numerical studies (Chen, Wang, and Xu 2023; Kang et al. 2022; Laurencin et al. 2011; Navasa, Yuan, and Sundén 2015) have been reported to investigate the temperature and heat generation inside the stack during operation. Given the impracticality of directly observing

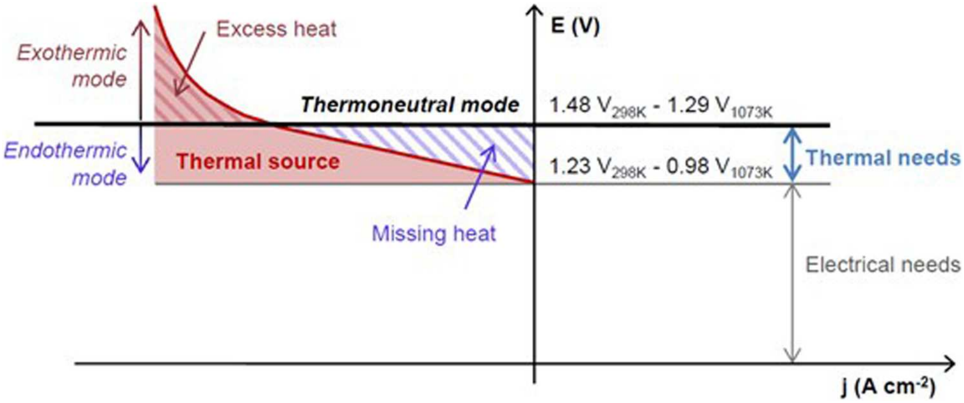

Figure 1. Operating mode of SOEC (Zhang et al. 2015).

gas flow, current density, and temperature at high operating temperatures, numerical simulation is a more viable alternative to experimental methods. One-dimensional simulations (Ni, Leung, and Leung 2007; Udagawa, Aguiar, and Brandon 2007), two-dimensional (Menon, Janardhanan, and Deutschmann 2014; Ni 2009), and three-dimensional (3-D) (Hawkes et al. 2009; Navasa, Yuan, and Sundén 2015; Xu et al. 2019) computational fluid dynamics (CFD) investigations have been carried out to investigate various operational parameters such as temperature (Kang et al. 2022; Navasa, Yuan, and Sundén 2015; Wang et al. 2018), voltage (Kang et al. 2022), steam flow rate (Cai et al. 2010), steam conversion(Chen, Wang, and Xu 2023; Laurencin et al. 2011), steam partial pressure (Chen, Wang, and Xu 2023), air flow rate (Barelli, Bidini, and Cinti 2018; Petipas, Brisse, and Bouallou 2017), flow configuration (Xu et al. 2017), and porosity (Weng et al. 2020).

Earlier work by Hawkes et al. (2009) and O'Brien, Stoots, and Herring (2010) developed a 3D model of solid oxide electrolysers, providing detailed insights into temperature profiles, Nernst and operating potentials, current density, gas composition, and hydrogen production across various operating conditions. Navasa, Yuan, and Sundén (2015), Zhang et al. (2021), and Kang et al. (2022) investigate the impacts of different operating voltages (1.1–1.5 V), operating temperatures (1073–1273 K), and flow configurations on the current density and temperature distribution of the cell. Xu et al. (2017) investigated the effect of flow configuration on cell performance and found that counter-flow resulted in a smaller operating temperature gradient compared to co-flow and cross-flow configurations, thereby improving cell durability. In addition, the uniformity of gas distribution inside a cell stack highly depends on the temperature distribution, temperature gradient, and heat flow across the cell stack. Wang et al. (2023) reported that the temperature gradient is the highest in cross-flow configurations, contributing significantly to the probability of failure due to degradation.

The Response Surface Method, commonly referred to as RSM, is a statistical and mathematical approach extensively employed to optimise and analyse the performance of fuel cells (Cui et al. 2024). This method enables the modelling of complex relationships among various operational parameters, including temperature (Barari, Morgan, and Barnard 2014; Tikiz and Taymaz 2016), pressure (Mojaver, Khalilarya, and Chitsaz 2019), current density(Roy, Samanta, and Ghosh 2020), and materials (Yan et al. 2019), as well as the cells' response variables, such as efficiency, hydrogen production rate, and degradation rate. By using experimental design and regression models, RSM helps to predict how these parameters impact cell performance, facilitating the optimisation of operating conditions to improve both efficiency and durability. This approach is particularly valuable in identifying interactions between different variables, as well as in refining operational conditions with a minimal number of experimental runs, making it a cost-effective strategy for studying and improving fuel cell systems (Ferrero et al. 2017).

Despite extensive studies on the impacts of operating conditions and electrochemical parameters on cell performance, comprehensive research that maps temperature distribution and predicts thermal gradients under varied operating conditions, which are key factors affecting fuel cell efficiency and durability, remains limited. This gap constrains the development of advanced thermal management strategies that could significantly improve both the efficiency and lifespan of SOECs. Although operating at thermoneutral voltage is beneficial, practical applications often deviate from this ideal due to material constraints, operational variability, and design limitations.

To the best of the author's knowledge, no previous study has employed Response Surface Methodology (RSM) to predict hotspot temperature in Solid Oxide Electrolyser Cells (SOECs). This study addresses existing challenges by investigating the influence of operating conditions, including voltage, temperature, steam mass fraction, and flow configuration, as well as microstructural and kinetic properties such as electrode porosity, and charge transfer coefficient, on the temperature distribution and hotspot formation near the thermoneutral point. A computational fluid dynamics (CFD) model of the SOEC was developed using ANSYS Fluent to simulate temperature distribution under various operational conditions. Central Composite Design (CCD) was implemented with MINITAB for RSM-based optimisation of critical parameters, including voltage, temperature, and steam mass fraction. This optimisation aimed to minimise hotspot formation, improve

SOEC efficiency, and enhance cell durability and longevity. This study addresses material degradation caused by thermal gradients, a key barrier to SOEC commercialisation, by optimising operating parameters to minimise temperature gradients, thereby improving durability and extending the lifespan of the cells.

2. Numerical model

2.1. Model description

Figure 2 presents a schematic representation of the geometry of SOEC. The geometry and parameters of the cell used in this study are summarised in Table 1.

In this study, the SOEC comprises the Nickel-Oxide/ Yttria-stabilized zirconia (NiO/YSZ) anode, Yttria-stabilized zirconia (YSZ) electrolyte, Lanthanum strontium manganite (LSM) cathode, and metal interconnectors. The material properties of the electrode, electrolyte, and interconnectors are based on Ghorbani and Vijayaraghavan (2018), is tabulated in Table 2.

2.2. Governing equations

The thermal conductivity, density, dynamic viscosity, and specific heat which was pre-defined by the ANSYS FLUENT (ANSYS 2023) were considered when solving for the porous domain.

The mass conservation equation for SOEC is

$$\nabla.(\rho\varepsilon\vec{v}) = S_m \tag{1}$$

where ε is porosity, the source term is $S_m = \sum_i S_{m,i}$ in the active zone (TPB) and zero in the inactive zone.

The momentum conservation equation is

$$\nabla.(\rho\varepsilon\vec{v}\,\vec{v}) = -\varepsilon\nabla p + \ \nabla\,(\varepsilon\mu\nabla\vec{v}) + S_M \tag{2}$$

where the source term $S_M = -\mu v/K$ in the porous electrode zone and zero in the gas channel, K indicates the permeability, which is dependent on the porosity of the porous electrode zone.

The material transportation equation is

$$\nabla.(\rho\varepsilon\vec{v}C_i) = -\nabla(\rho D_{i,eff}C_i) + \ \nabla S_{s,i} \tag{3}$$

where $D_{i,eff}$ denotes the effective diffusion coefficient of materials I, the source term is $S_{s,i} = M_i.j/n_eF$ in the TPB and zero in the inactive zone, j denotes the current density (A/m^2).

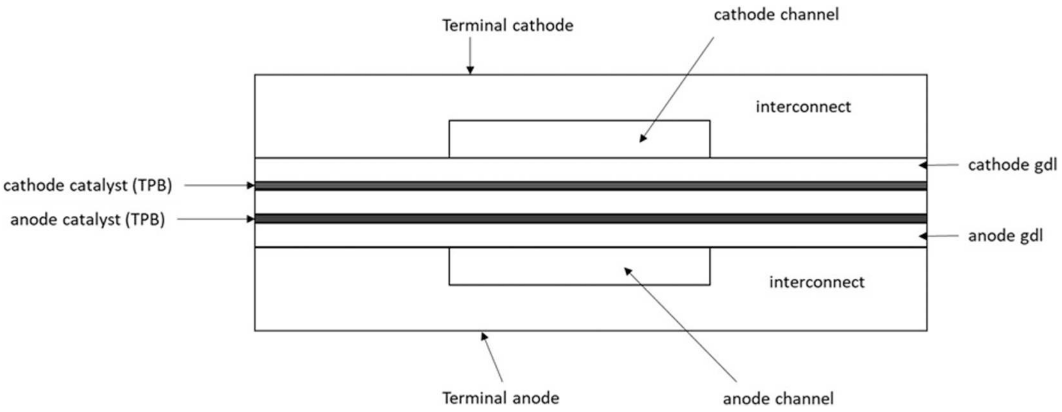

Figure 2. SOEC model description.

Table 1. Geometry and operational parameters.

Geometry and operational parameters	Value	Units
Operating temperature	1073	K
Operating pressure	1	bar
Length and width	100	mm
Anode diffusion layer thickness	5	mm
Anode TPB layer thickness	0.1	mm
Electrolyte thickness	1	mm
Cathode TPB layer thickness	0.1	mm
Cathode diffusion layer thickness	1	mm
Steam and Air channel height	10	mm
Steam and Air channel width	50	mm
Open circuit voltage (OCV)	1.0	V
Anode exchange current density	2000	A/m^2
Cathode exchange current density	7500	A/m^2

Porosity modifies the effective diffusion oefficient $D_{i,eff}$ in the porous medium, influencing the transport of species. The inclusion of ε accounts for the reduced transport pathways in the porous structure.

The energy conservation equation is

$$\nabla.(\rho\varepsilon\vec{v}c_pT) = \nabla(k^{eff}\nabla T) + S_T \tag{4}$$

where k^{eff} denotes the effective heat conductivity coefficient, the source term $S_T == j^2/\sigma + j(\eta_{act} + T\nabla S/2F)$ in the TPB and $S_T = j^2/\sigma$ in such zones as the gas channel, electrode, and current collector.

The electrolyte governing equation is

$$\sigma_0^{eff}\nabla\varphi_{mem} = j_0 \tag{5}$$

where σ_0^{eff} denotes the effectiveness of O^{2-} diffusion rate (Ω^{-1}); φ_{mem} indicates ion potential (V)

The current collector governing equation is

$$\sigma_{sol}\nabla\varphi_{sol} = j \tag{6}$$

where σ_{sol} denotes the conductivity of the current collector (Ω^{-1}).

The governing equations and corresponding source term is summarised in Table 3 below.

2.3. Boundary conditions

The inlet and outlet boundary conditions and cell conditions (Navasa, Yuan, and Sundén 2015) are summarised in Tables 4 and 5.

This study operates under the assumptions of a steady-state condition, laminar flow, an incompressible gas, negligible radiation heat transfer, and an isotropic, homogeneous electrode.

Table 2. Materials properties of the electrode, electrolyte and interconnector (Ghorbani and Vijayaraghavan 2018).

Materials properties	Anode NiO/YSZ	Electrolyte YSZ	Cathode LSM	Interconnector Metal
Specific heat (J/kg.K)	450	450	450	450
Thermal conductivity (W/m.K)	10	2	11	72
Electron conductivity (1/Ωm)	333,330	–	7973	1.5×10^7
Density (kg/m^3)	6500	5480	5620	8900
Tortuosity	3	–	3	
Anode contact resistance (Ωm^2)	–	–	–	1×10^{-7}
Cathode contact resistance(Ωm^2)	–	–	–	1×10^{-8}

Table 3. Governing equations.

Governing equation	Source term	
Continuity equation	Except TPBs $S_m = 0$	TPB $S_m = \sum_i S_{m,i}$
Momentum equation	Channels $S_M = 0$	TBPs and diffusion layer $S_M = -\mu v/K$
Energy equation	Diffusion layer, electrode, interconnects $S_T = j^2/\sigma$	TBP $S_T = j^2/\sigma + j(\eta_{act} + T\nabla S/2F)$
Species equation	Except TPBs $S_{s,i} = 0$	TBPs $S_{s,i} = M_i.j/n_e F$
Charge transport	Except TPBs $= 0$	TBP = j

Table 4. Boundary conditions.

Boundary conditions	Location	Value		Unit
Mass flow rate	Inlet steam channel	Mass flow rate inlet ($\dot{m}_{H_{2O/H_2}}$)	1.6×10^{-5}	kg/s
		Temperature	1073–1273	K
		H_2O mole fraction	0.1-0.9	
		H_2 mole fraction	0.1-0.9	
	Inlet air channel	Mass flow rate ($\dot{m}_{O_{2/N_2}}$)	8.66x 10^{-6}	kg/s
		Temperature	1073–1273	K
		O_2 mole fraction	0.21	
Pressure outlet	Outlet steam channel	–	-	-
	Outlet air channel	–	-	-
Wall	Terminal Anode	Specified electric potential	0	V
	Terminal Cathode	Specified electric potential	1.1-1.5	V
	All faces	Constant temperature	1073–1273	K

Table 5. Cell zone condition.

Zone name	Zone type	Porous
Anode CC	Solid	–
Cathode CC	Solid	–
Anode GDL	Liquid	Yes
Cathode GDL	Liquid	Yes
Steam channel	Liquid	No
Air channel	Liquid	No
Electrolyte	Liquid	Yes
TPB	Liquid	Yes

2.4. Solution method

A three-dimensional model of a planar SOEC is developed to investigate the performance of the cell using ANSYS FLUENT 2024R with Addon Module 3 Fuel Cell and Electrolysis. A three-dimensional (3D) model was chosen for this study to capture the detailed spatial variations in temperature, flow dynamics, and reaction kinetics within the Solid Oxide Electrolyser Cell (SOEC). The most important thing to note in the add-on module is that the anode and cathode are configured similarly to those in SOFC, with the anode serving as the fuel electrode and the cathode as the air electrode.

The study used the semi-implicit method for pressure-linked equations (SIMPLE) solver with a first-order discretisation scheme for all equations, except for pressure, where a standard scheme was used, and the Green Gauss cell-based method for diffusive fluxes (Navasa, Yuan, and Sundén 2015). The solver's sensitivity to species equations necessitates defining an appropriate under-relaxation factor for each equation for the solution to converge, as the default settings are inadequate. If the solution exhibits fluctuating behaviours, the bi-conjugate gradient stabilised method (BGSTAB) is used to achieve stable solutions. The residuals for the continuity equation, velocity, and species were set to 10^{-4}, while the residual for the energy equation was set to 10^{-9} for greater accuracy. Apart from the residual, the current density, species mass fluxes, and residual were monitored for convergence (Arvay et al. 2012).

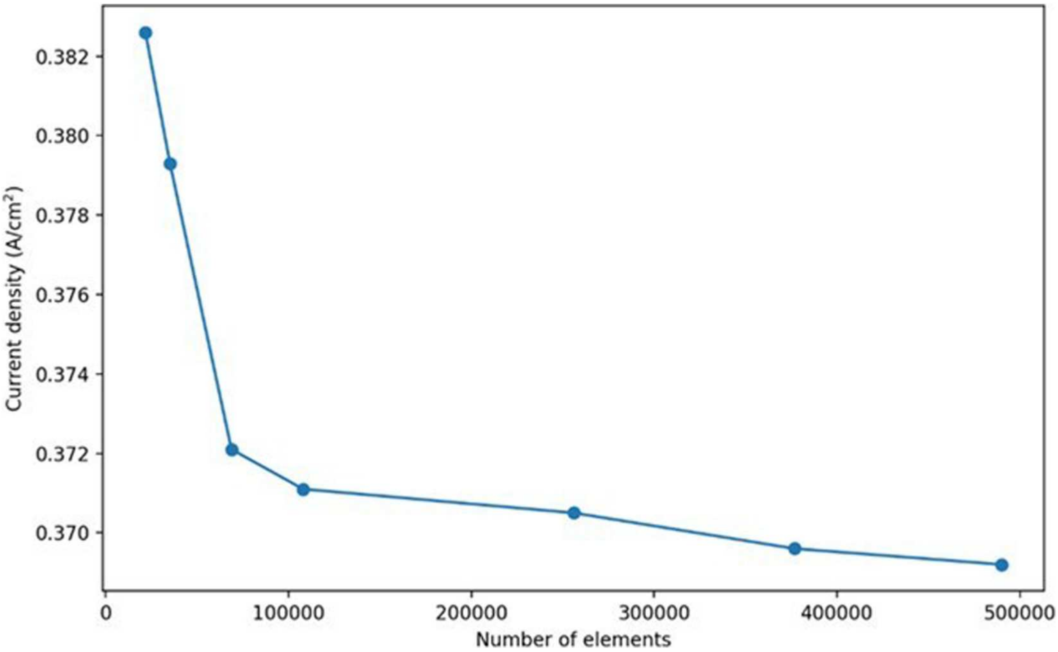

Figure 3. Mesh dependency study.

2.5. Mesh dependency studies

Hexahedral mesh with 21,780, 68,850, 107,991, 256,000, and 490,000 elements were used in the mesh dependency studies as shown in Figure 3. The 256,000 elements were chosen for this study as the results showed variations around 0.8% relative to the finer mesh.

2.6. Model validation

The current model was validated against experimental data from Liu et al. (2016) and the numerical results of Kang et al (Kang et al. 2022) under identical operating conditions. The current simulation results show an average variation of approximately 9.5%, reflecting a strong agreement with both studies, as illustrated in Figure 4.

3. Response surface methods

3.1. Response surface methodology

Response Surface Methodology (RSM) is an optimisation technique that uses mathematical and statistical tools to develop empirical models and identify the optimal values of variables for maximising or minimising a response (Nguyen et al. 2023). e. It captures direct impacts and interactions between variables by representing them through two-dimensional or three-dimensional plots. The response surface is expressed as

$$y = f(x_1, x_2, x_3, \ldots\ldots, x_n) \tag{7}$$

where y is the system's response and x_n is the set of influencing factors.

This study utilised Response Surface Methodology (RSM) to determine the optimal operating conditions for minimising the temperature gradient in Solid Oxide Electrolyser Cells (SOECs) during operation. RSM was employed to complement Computational Fluid Dynamics (CFD)

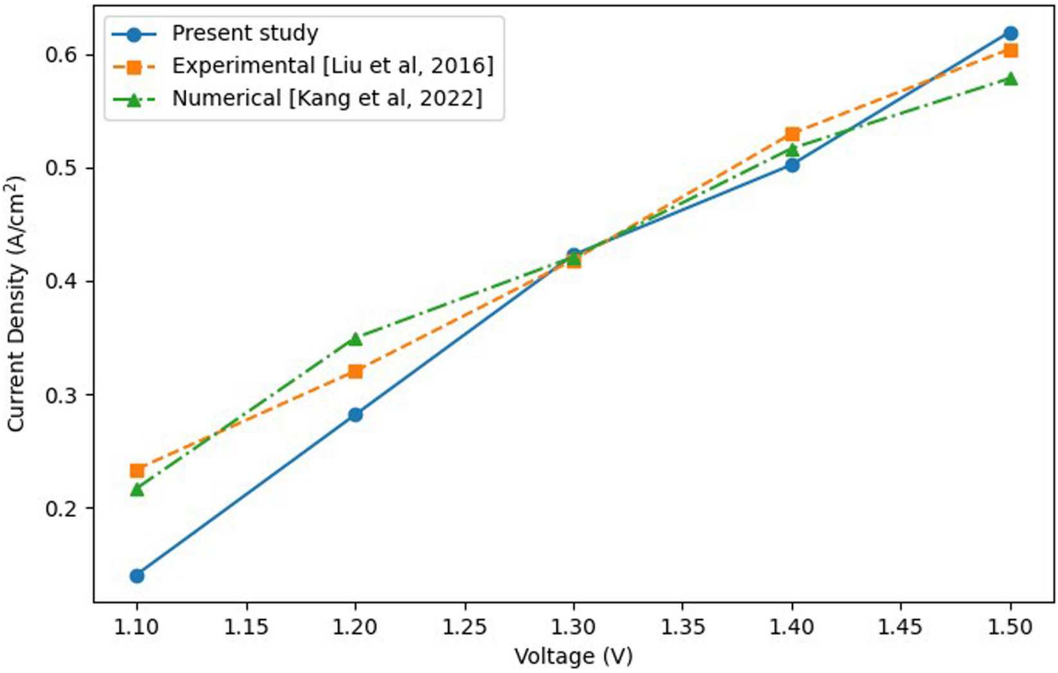

Figure 4. Comparison of the polarisation curve for the present study with experimental (Mojaver, Khalilarya, and Chitsaz 2019) and numerical study (Kang et al. 2022).

simulations by providing an efficient statistical approach to approximate the relationships between input parameters (e.g. voltage, temperature, and steam mass fraction) and output responses. While CFD offers detailed insights into the thermal, flow, and electrochemical behaviours of the system, it is computationally expensive for exploring a wide range of parameter combinations. By reducing the need for extensive CFD runs, RSM enables the identification of optimal conditions with greater efficiency, balancing detailed analysis with computational practicality.

Central Composite Design (CCD) and Box–Behnken Design (BBD) are both widely used experimental designs for response surface methodology (RSM), aimed at optimising processes by exploring the relationships between input factors and responses (Benedetti, Caponigro, and Ardini 2022). While BBD focuses on midpoints and avoids extreme parameter values, CCD is more flexible as it incorporates axial points that extend beyond the factorial levels, allowing for a more comprehensive exploration of the design space (Sharafinia, Farrokhnia, and Ghasemian Lemraski 2022). This feature makes CCD particularly suitable for studying systems with potential extreme conditions.

In this study, CCD was chosen over BBD due to its ability to handle a wide range of operating conditions and its robustness in capturing the effects of extreme values, such as high voltages or temperatures, on the thermal and operational behaviour of Solid Oxide Electrolyser Cells (SOECs). By incorporating centre and axial points, CCD enables the development of precise second-order polynomial models, leading to improved accuracy in optimisation and prediction (Breig and Luti 2021). These advantages made CCD the more appropriate choice for achieving the objectives of this study.

The primary independent variables for the experimental design were selected based on their significant impact on fuel cell performance, as determined through parametric studies. These variables included temperature, voltage and steam mass fraction, as they directly impact the electrochemical and thermal behaviour of the cell. A Central Composite Design (CCD) approach was employed to systematically generate the process variable set. This included factorial points to estimate main effects and interactions, as well as axial points to capture curvature in the response surface. The levels for each variable were carefully determined by considering both practical operational ranges and theoretical boundaries, ensuring a comprehensive exploration of their effects while maintaining relevance to real-world applications. Each input factor was evaluated on a five-level scale, including axial points (-α and +α), factorial points (−1 and +1), and a central point (0), as defined by the Central Composite Design (CCD).

ANSYS simulations were performed to calculate the response parameter values at the selected design points. The resulting data were used to construct a response surface, which was evaluated for adequacy using statistical goodness-of-fit criteria. If the model was found to be not significant during the analysis of variance (ANOVA), adjustments were made to the design by modifying the levels of the independent variables and expanding the experimental range. These modifications enhanced the model's ability to accurately capture the response variability and achieve a statistically significant fit.

As illustrated in Figure 5, this iterative refinement process is represented by the feedback loop, ensuring that the Central Composite Design (CCD) is systematically adjusted to develop a well-fitted regression surface model and enable effective response optimisation. The primary output variable in the RSM implementation was the hotspot temperature within the cell. This variable was chosen for its critical role in understanding the thermal behaviour of the system and its impact on performance and durability.

Once validated, the response surface models were used for optimisation through Response Surface Methodology (RSM). The optimisation process was conducted using the Response Optimiser

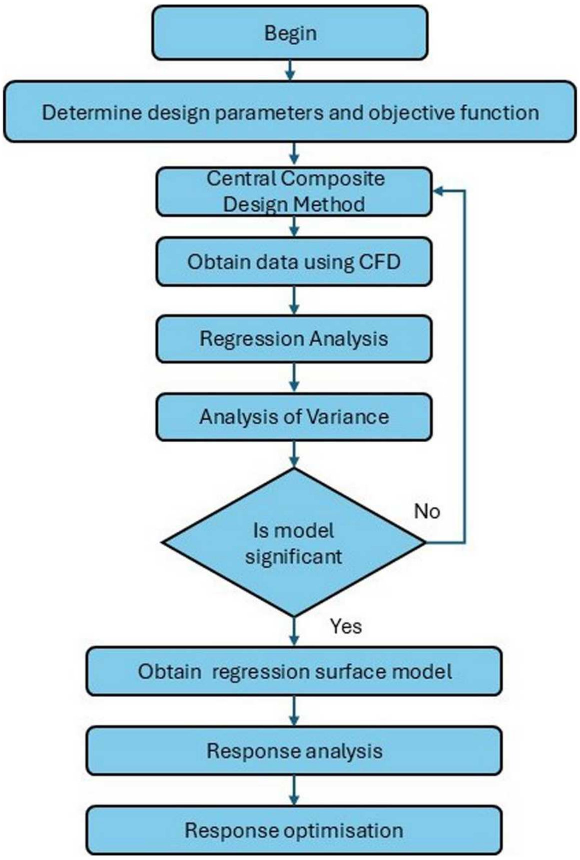

Figure 5. Response Surface Method (RSM) Methodology.

Table 6. Design variables.

			Level			
Variables	Symbols	−2	−1	0	+1	+2
Operating temperature (K)	T	1073	1123	1173	1223	1273
Operating voltage (V)	V	1.1	1.2	1.3	1.4	1.5
Steam Mass Fraction	SMF	0.5	0.6	0.7	0.8	0.9

in MINITAB statistical software, which calculated response desirability. The optimal solution was determined when the desirability value reached its maximum, ensuring the best combination of operating conditions to minimise thermal gradients and hotspot formation.

3.2. Design variables and optimisation process

In this study, operating voltages, operating temperature and steam mass fraction were selected as independent parameters that affect the temperature distribution of the SOEC. Table 6 below presents a list of factors used in this CCD, with levels −1 and +1 representing the lower and upper limits of the variables, level 0 corresponding to the middle limit, and axial points (−2 and +2). The total number of design points (N) required for a three variable (n = 3) factorial experiment, including n_c as the number of centre point ($n_c = 6$) is determined using (Sahu, Acharya, and Meikap 2009)

$$N = 2^n + 2n + n^c = 2^3 + (2)(3) + 6 = 20 \tag{8}$$

Centre point replication improves prediction capability near the centre of the factor space (Xu et al. 2023).

Objective functions serve a variety of purposes, such as maximising or minimising outcomes, or achieving specific target values. The objective function (G) of this study is the hot spot temperature (HST). The hot spot temperature of the cell was simulated in ANSYS Fluent based on 20 designs produced by CCD. The results for the CCD are provided in Table 7 below.

Table 7. Central composite design of operating parameters.

	Independent variables			Response
Case number	Operating temperature, T (K)	Operating voltage, V (V)	Steam mass fraction, SMF	Hot spot temperature, HST (K)
1	1223	1.4	0.6	1233
2	1123	1.2	0.8	1124
3	1123	1.2	0.6	1124
4	1173	1.3	0.5	1176
5	1223	1.2	0.6	1224
6	1173	1.3	0.7	1175
7	1223	1.4	0.8	1234
8	1173	1.3	0.7	1175
9	1173	1.5	0.7	1189
10	1173	1.3	0.7	1175
11	1173	1.3	0.7	1175
12	1173	1.3	0.7	1175
13	1173	1.3	0.7	1175
14	1273	1.3	0.7	1279
15	1173	1.3	0.9	1177
16	1173	1.1	0.7	1173
17	1223	1.2	0.8	1224
18	1123	1.4	0.8	1129
19	1073	1.3	0.7	1074
20	1123	1.4	0.6	1129

RSM constructed quadratic polynomial equations to predict the hot spot temperature based on the independent parameters and interaction effects on these variables. The quadratic polynomial function, which includes linear, squared, and interaction terms (Chen et al. 2023), is given by:

$$G = a_0 + \sum\nolimits_{i=1}^{k} a_i x_i + \sum\nolimits_{i=1}^{k} a_{ii} x_i^2 + \sum\nolimits_{i=1}^{k} a_{ij} x_i x_j + \varepsilon_i \tag{9}$$

where a_0, a_i, a_{ii} and a_{ij} represent the intercept of the regression coefficient, the linear impact of x_i, the quadratic impact of x_i, and the linear interaction impact between x_i and x_i. To verify the validity and reliability of the regression model, analysis of variance (ANOVA), degrees of freedom (DF), and regression coefficients, along with P and F values were assessed. Response surface analysis was carried out to illustrate interactions between pairs of design parameters, using surface and contour plots to evaluate the influence of independent variables on the response. Optimal design parameters were identified using the Pareto optimal solution.

4. Results and discussion

The performance and temperature distribution of SOEC highly depend on its operating parameters, which directly influence their efficiency, durability, and overall effectiveness of the electrochemical process. This study varied the operating voltage and temperature to examine their impacts on cell performance, while also investigating the effects of flow configurations, porosity, and charge transfer coefficients under thermoneutral mode.

4.1. Parametric studies

4.1.1. Impacts of operating voltage

The operating voltage is crucial in determining the endo-exothermicity of the stack. In this study, the operational voltage was varied within the range of 1.1 to 1.5 V at 1073 K to illustrate three modes of SOEC operation which are endothermic, exothermic, and thermoneutral mode. Figure 6 shows

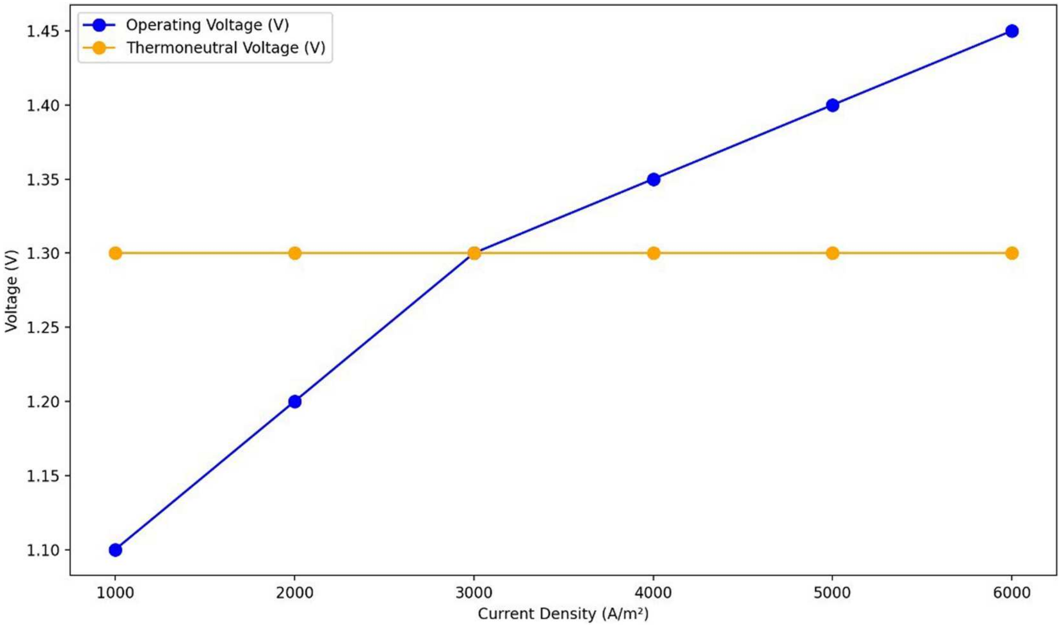

Figure 6. Impacts of operating voltage on the polarisation curve.

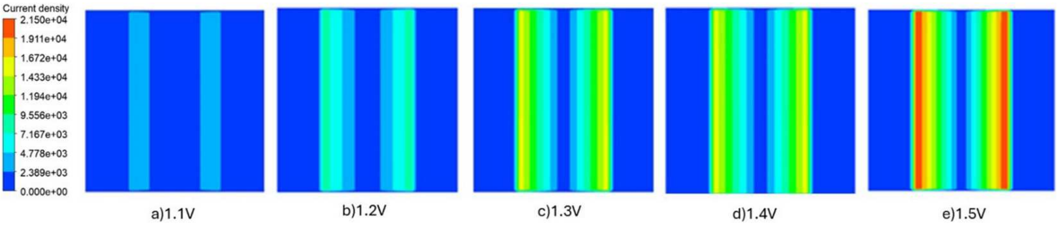

Figure 7. Current density at 1073 K under different operating voltages (a) 1.1 V, (b) 1.2 V, (c) 1.3 V, (d) 1.4 V and (e) 1.5 V at the electrode-electrolyte interface.

the polarisation curve for the cell. The performance of SOEC is characterised by the polarisation curve as it illustrates the correlation between current density and the voltage across the cell which provides insight into the total losses observed over the applied current (Sriram Srinivas et al. 2023). The current density is observed to increase linearly with rising operating voltage, primarily due to higher irreversible losses (Koh, Yoon, and Oh 2010). Operating at higher voltages increases the cell's ohmic resistance, leading to greater heat dissipation and resistive losses. As the voltage rises, the activation overpotential also grows, requiring more energy to overcome the reaction barriers. The concentration overpotential increases because of reduced reactant availability at the electrode surface. As the operating voltage increases, these factors and the extra heat generated result in higher irreversible energy losses. During operation, a high current density is favourable for increasing the rate of total energy production (Min et al. 2021); therefore, minimising this resistance is essential for achieving high current-density operation (Sriram Srinivas et al. 2023). The current density distribution is significantly affected by the levels of activation overpotential and Nernst potential (Hawkes et al. 2009). It is observed that the operation mode of SOEC shifts from endothermic to exothermic as the current density changes at 1.3 V.

Figure 7 shows the current density distribution at the interface of the electrode and electrolyte. The current density is observed to be highest near the interconnector rib along the steam channel and decreases toward the centre. The low current density observed at the centre is due to the absence of direct contact between the electrode and the interconnect beneath the steam channel (Zhang et al. 2021). A similar current density distribution is reported by Navasa et al (Navasa, Yuan, and Sundén 2015) which identified that the peak current density values are predominantly found in the continuous areas at the interface of the channel and the side interconnects. This is due to the higher electron concentrations in the solid regions and the diffusion of electrons from the solid interconnectors to the porous layers, and subsequently to the reaction sites.

Figure 8 illustrates the temperature distribution of the fuel cell operating in endothermic mode at 1.1 V, which is below the thermoneutral voltage. In this mode, the temperature decreases along the direction of steam flow. Xu et al. (2019) attributed this reduction to a higher rate of heat absorption compared to heat diffusion. Operating in endothermic mode requires the cell to absorb heat from

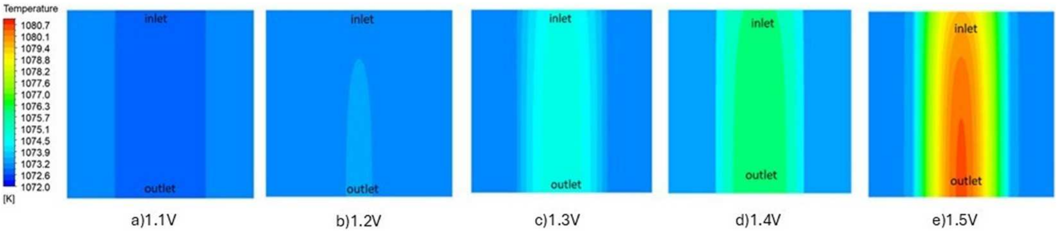

Figure 8. Temperature distribution at 1073 K under different operating voltages (a) 1.1 V, (b) 1.2 V, (c) 1.3 V, (d) 1.4 V and (e) 1.5V.

its surroundings to sustain the electrochemical reaction, as the electrical energy supplied is less than the reaction's enthalpy. At low voltages, this additional heat input is essential to drive the electrochemical processes effectively. At 1.3 V, the outlet temperature is observed to be the same as the inlet temperature, indicating an equilibrium where the supplied electrical energy equals the reaction's enthalpy, resulting in no net heat exchange. In contrast, at 1.5 V, the fuel cell operates in exothermic mode, as the operating voltage exceeds the thermoneutral voltage. In this case, the electrical energy supplied surpasses the heat required for the reaction, releasing the excess energy as heat. The resulting temperature increase near the steam channel outlet is consistent with findings reported by (Chen, Wang, and Xu 2023; Kang et al. 2022) which emphasises the importance of heat removal to maintain a uniform temperature distribution across the cell. The temperature rise at higher voltages is primarily attributed to the dominance of electrical ohmic resistance over the reaction's enthalpy demands (Lu et al. 2024). This transition from endothermic to exothermic operation reflects the balance between the supplied electrical energy and the thermal energy demands of the electrochemical process.

Figure 9 demonstrates that hydrogen production increases with the rise in operating voltage, leading to a higher current density. Since current density is directly correlated with the rate of hydrogen production, higher current density results in increased consumption of steam for hydrogen production (Kamkeng and Wang 2022). However, the increase in current density raises the steam channel outlet temperature due to a higher rate of electrochemical reaction. At higher operating voltages, especially above the thermoneutral voltage, the heat generated by the exothermic reaction can be utilised to reach the operating temperature, reducing the need for additional heat sources and potentially significantly improving the efficiency of hydrogen production (Fang et al. 2024). Although the operating voltage plays a crucial role in determining the hydrogen production rate, it presents a trade-off in terms of efficiency, as an increase in operating voltage leads to a decrease in the efficiency of the electrolysis process (Hauch and Blennow 2023). This is mainly attributed to the area-specific resistance (ASR) (Graves et al. 2011) which accounts for the combined effects of all loss mechanisms in the electrolysis stack, including ohmic losses, activation overpotentials, and concentration overpotentials (O'Brien, Stoots, and Herring 2010). In addition, the increase in operating voltage also raises thermal stress in the SOEC due to the rise in cell temperature, emphasising the importance of effective temperature control to increase the cell lifespan (Lu et al. 2024).

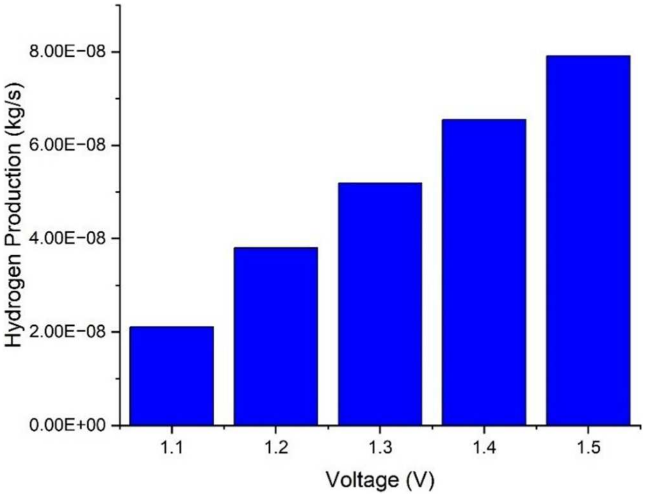

Figure 9. Hydrogen production based on voltage.

4.1.2. Impacts of operating temperature

Temperature is another crucial operating condition, given its influence on both thermodynamics and kinetics. Higher temperatures can enhance transport processes in fuel cells, including charge transfer, charge conduction, and mass transport while decreasing internal resistance and electrical demand, which results in improved efficiency (Samavati et al. 2017). The voltage of 1.1, 1.3, and 1.5 V were chosen as the base case studies to represent the endothermic, exothermic, and near thermo-neutral voltage modes.

Figure 10 illustrates the impacts of operating temperature on the polarisation curve of the cell. The current density is 1.6A/m^2, 2.9, and 4.5 A/m^2 at 1073, 1173, and 1273 K respectively. The increase in operating temperature leads to a higher current density, due to favourable thermodynamics, fact reaction kinetics (Mahmood et al. 2015), and a decrease in the activation potential (Chen, Wang, and Xu 2023). The current density demonstrates a linear increase with temperature, consistent with findings reported by (Shimada et al. 2019; Zhang et al. 2022). The current density rises by 64% when the temperature increases from 1073 to 1273 K. High operating temperatures result in decreased activation resistance by enhancing the conductivity of the electrolyte ionic conductor, thereby increasing exchange current density and reducing contact losses and ohmic resistance (Chen, Wang, and Xu 2023; Ni, Leung, and Leung 2007). However, Chen, Wang, and Xu (2023) observed that extended operation at high temperatures causes fine-grained particles in the fuel electrode to agglomerate, reducing the number of active sites and negatively affecting both cell performance and durability.

Figure 11 shows the impacts of temperature on the current density. The operating temperature has a significant impact on the current density, as it lowers the reversible voltage and reduces other irreversible losses (Kang et al. 2022). The maximum current densities for 1073, 1173, and 1273 K are 1.24×10^4 A/m^2, 2.45×10^4 A/m^{2,} and 3.99×10^4 A/m^2 respectively. An increase in temperature enhances the reaction rate by increasing the thermal energy provided to the system and reducing the required electrical energy (Gibb's function) (Xu et al. 2019). At higher temperatures, sufficient kinetic oxygen transport is facilitated, leading to better performance, while conversely, a decrease in temperature increases the electrolyte's resistance to ionic flow (Weng et al. 2020). A similar current

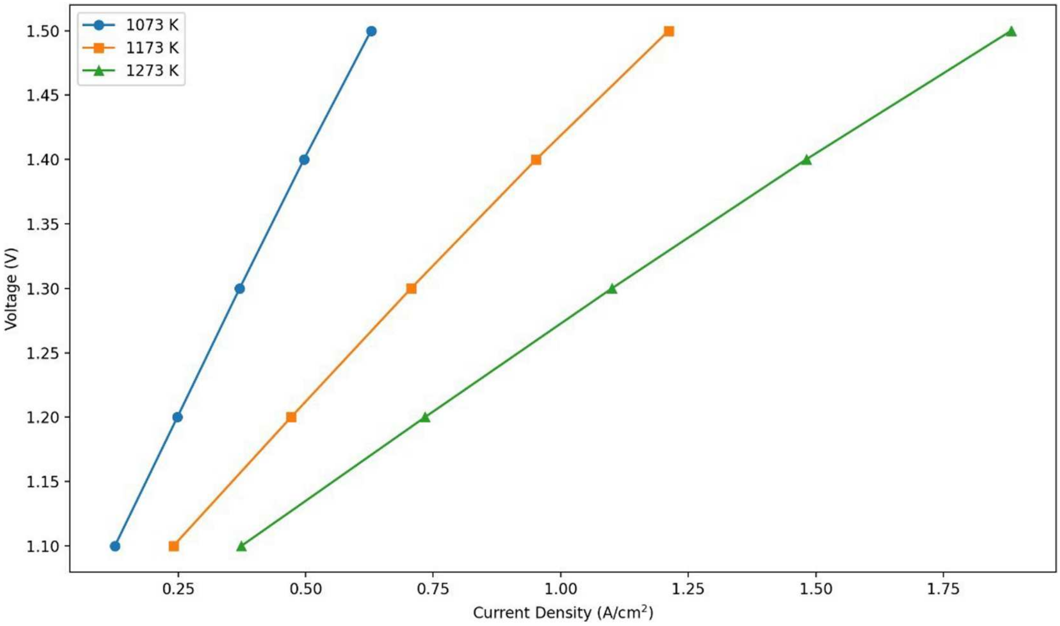

Figure 10. Impacts of operating temperature of 1073, 1173 and 1273 K on the polarisation curve.

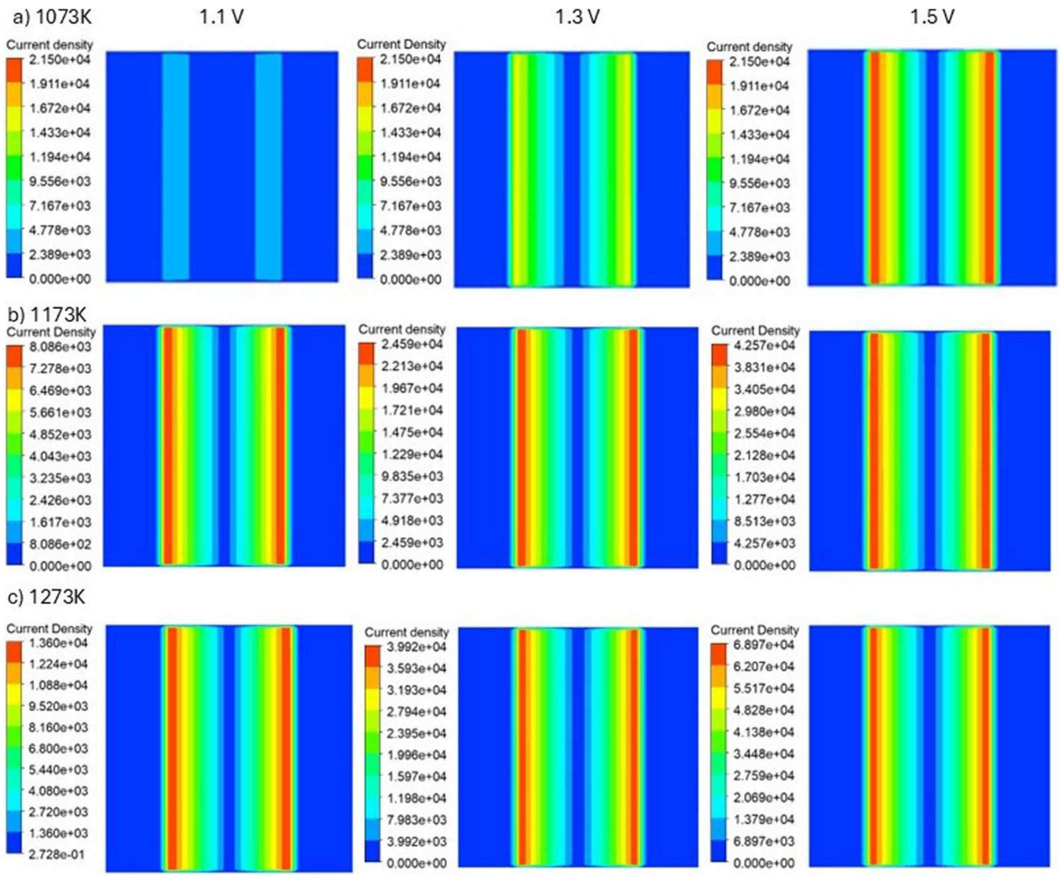

Figure 11. Impacts of the operating temperature on current density at the electrode-electrolyte interface: (a) 1073 K, (b) 1173 K, and (c) 1273 K, at operating voltages of 1.1, 1.3 and 1.5V.

density profile as in Figure 7 is obtained for the current density where the peak values of current density occurred under the rib between the channel and the interconnectors. The mass transfer under the rib could be enhanced by evenly distributing the steam in the electrochemical active zone through grooves and rib-finned interconnectors. This leads to a decrease in activation and concentration polarisation, thereby enhancing the overall cell performance (Fu et al. 2021).

Figure 12 depicts the impacts of operating temperatures on the temperature distribution. Weng et al. (2020) found that the efficiency of the cell was affected not only by operational temperatures but also by the temperature profile within the cell. When operating at 1.1 V, the temperature is seen to decrease by 3 K towards the fuel outlet. The primary reason for the temperature decrease in the direction of steam flow at 1.1 V is related to the endothermic nature of the electrochemical reactions occurring in the SOEC. At this voltage, the electrolysis process absorbs heat from the surroundings because it requires energy input to drive the endothermic reaction, where steam is converted into hydrogen and oxygen (Lang et al. 2020). As the steam flows through the cell and undergoes electrolysis, it absorbs heat from the cell, causing a drop in temperature in the direction of the steam flow (Lang et al. 2020). This absorption of heat leads to a temperature decrease as the steam progresses through the cell.

The temperature remains constant at 1.3 V as at the thermoneutral voltage, the heat generated by the Joule effect offsets the heat consumed by the reactions, resulting in a constant temperature (Grondin et al. 2010). On the other hand, when the cell operates at 1.5 V, the

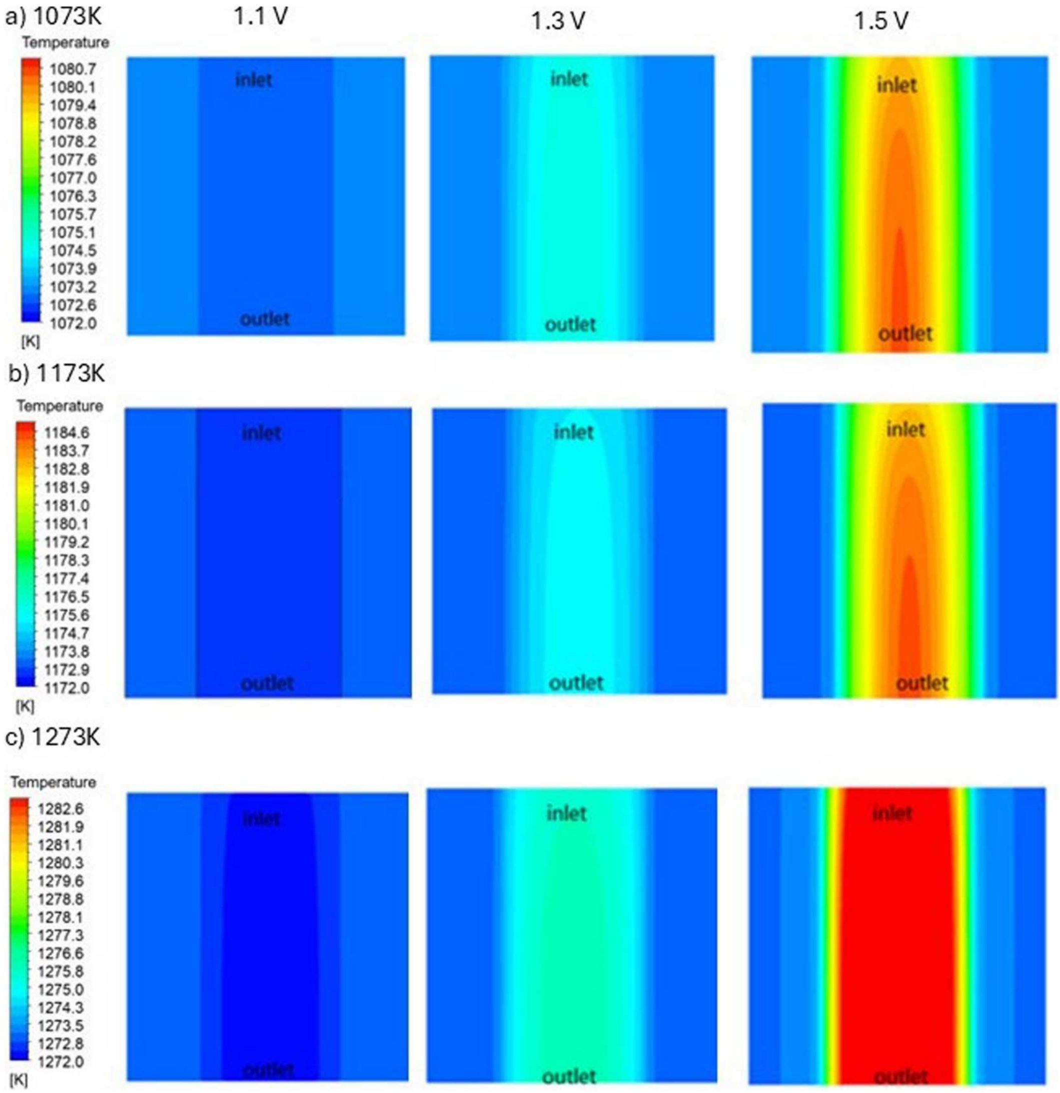

Figure 12. Impacts of the operating temperature on temperature distribution at the electrode-electrolyte interface: (a) 1073 K, (b) 1173 K, and (c) 1273 K, at operating voltages of 1.1, 1.3 and 1.5V.

temperature increases by 6 K, 11 K, and 15 K towards the fuel outlet for operating temperatures of 1073, 1173, and 1273 K respectively. It is observed that higher operating temperatures result in an increased thermal gradient inside the cell. This is primarily due to the reduction of the ohmic overpotentials due to a rise in proton conductivity, activation overpotentials due to a rise in reaction rates, and concentration overpotentials due to the increase in the diffusion rate of gases in porous materials (Namwong et al. 2016). However, high operating temperatures result in more rapid degradation of materials (Gaikwad et al. 2023) due to the coarsening, sintering, and migration of Ni which decreases the active TPB density. High operating temperature limits the material requirements of the electrode and electrolyte (Xu et al. 2023) and induces temperature variations which leads to thermomechanical stresses in the stack which leads to device failure (Chen et al. 2023). The fragile ceramic materials used in the cell are prone to failure under high-temperature gradients caused by sudden changes in loads (Xu et al. 2023). In addition, the boundary region between the cathode electrode and electrolyte experiences the most significant mismatches in thermal expansion coefficients, resulting in delamination due to atom diffusion across this boundary (Gaikwad et al. 2023).

Figure 13 shows that the hydrogen production rate increases from 5.19×10^{-8} kg/s to 1.4×10^{-7} kg/s when the temperature rises by 200 K at 1.3 V. A study by Ni, Leung, and Leung (2007) reported that the average current density rises linearly with hydrogen production. While raising the operating temperature enhances cell performance by increasing both current density and hydrogen production, it also results in a higher thermal gradient within the cell, which accelerates degradation mechanisms.

4.1.3. Impacts of steam mass fraction

Due to the oxidising environment created by steam at high temperatures, hydrogen recirculation mixed with steam at the inlet temperature is essential to mitigate this condition. Air, typically comprising 79% nitrogen and 21% oxygen, is used as the inlet stream for the air channel at the anode electrode. The effects of steam mass fraction at 1073 and 1.3 V are illustrated in Figure 14. It can be observed that current density rises with an increase in steam mass fraction. A similar trend was reported by Zhao, Lin, and Zhou (2022) which stated that the steam conversion rate increases as the steam mass fraction increases, driven by the higher activation potential.

Increasing the steam mass fraction at the fuel inlet leads to higher hydrogen production at the fuel outlet, as shown in Figure 15. This observation is consistent with the findings of Koh, Yoon, and Oh (2010), demonstrating that the steam mass fraction at the fuel inlet influences both hydrogen production and the Nernst voltage of the cell. However, changes in the steam mass fraction do not notably impact the temperature distribution within the system. The temperature distribution at various steam mass flow rates, observed at 1073 and 1.3 V, is similar to the pattern shown in Figure 12.

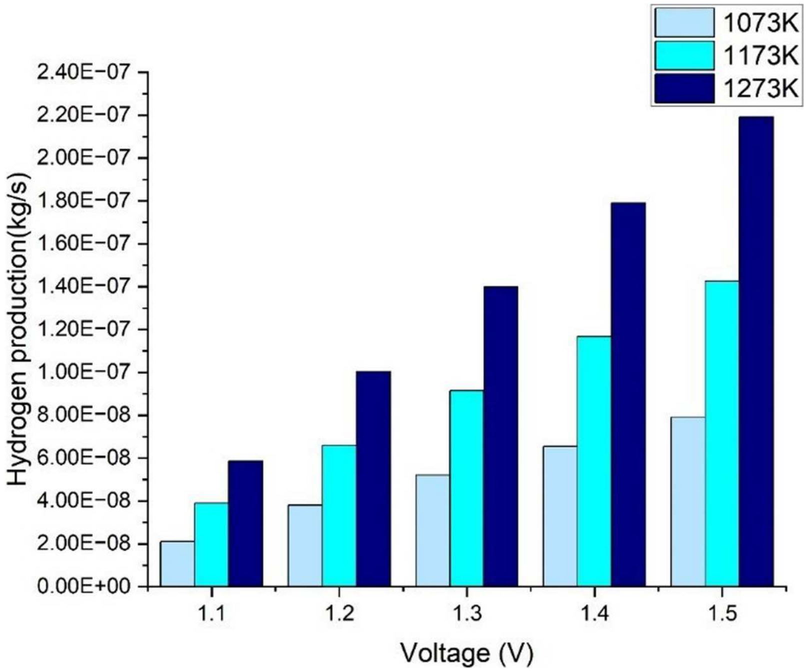

Figure 13. Hydrogen production based on temperature.

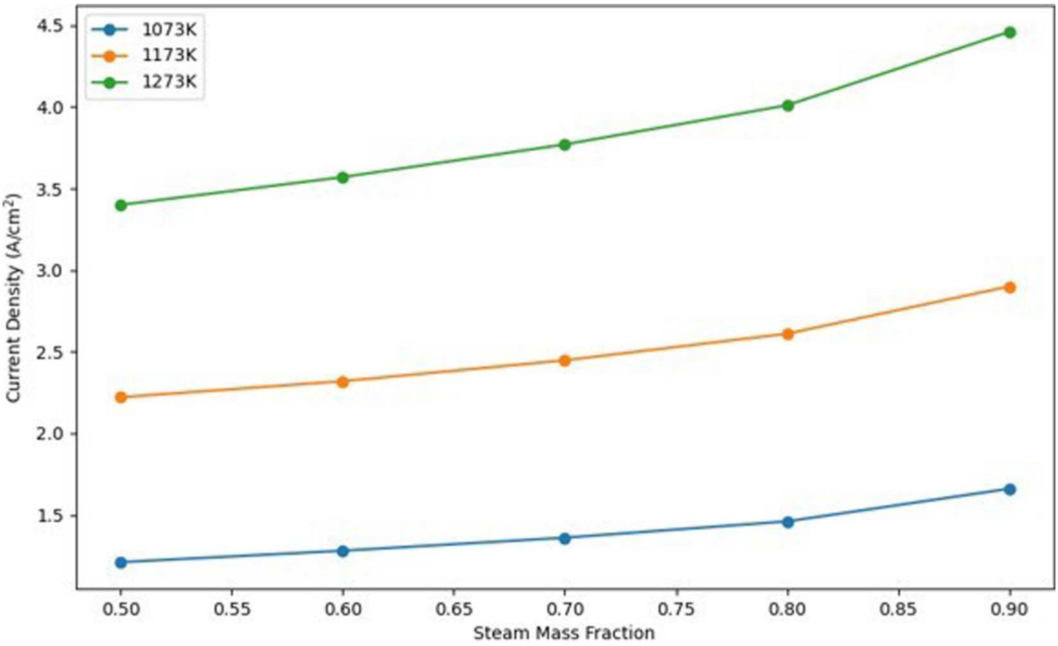

Figure 14. Impacts of the Steam Mass Fraction at 1073 K and 1.3V.

4.1.4. *Impacts of flow configurations*

The efficiency and performance of SOEC are greatly affected by steam flow configurations, which impact temperature distribution, current density, and consequently affect thermal, electrochemical, mechanical, and electrical aspects of the cell (Xu et al. 2017). Figures 16, 17, 18 show the

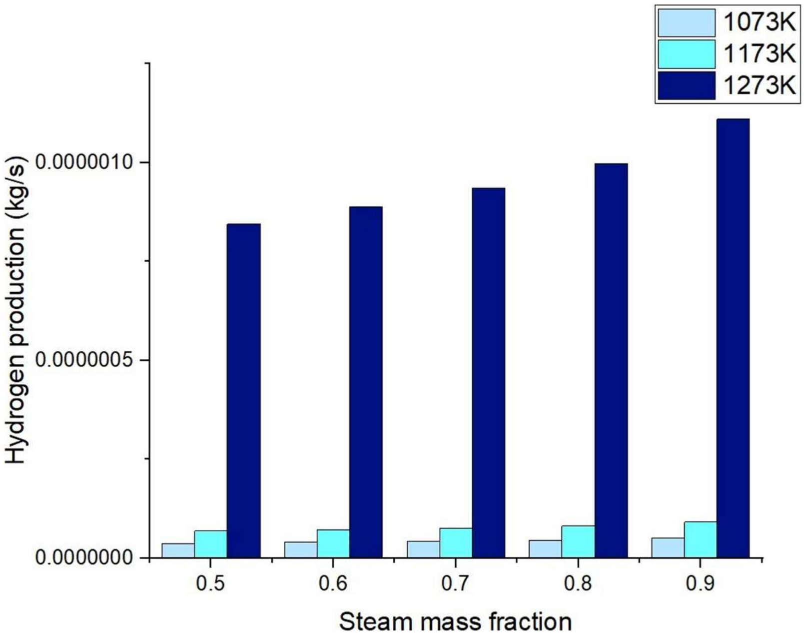

Figure 15. Impacts of steam mass fraction on hydrogen production at 1073 K and 1.3V.

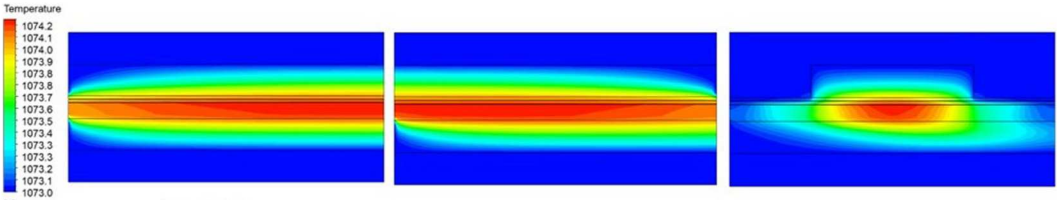

a) Parallel flow b) Counter flow c) Perpendicular flow

Figure 16. Temperature distribution across the cell components at 1073 K and 1.3 V at different flow configurations (a) parallel flow, (b) counter flow, and (c) perpendicular flow.

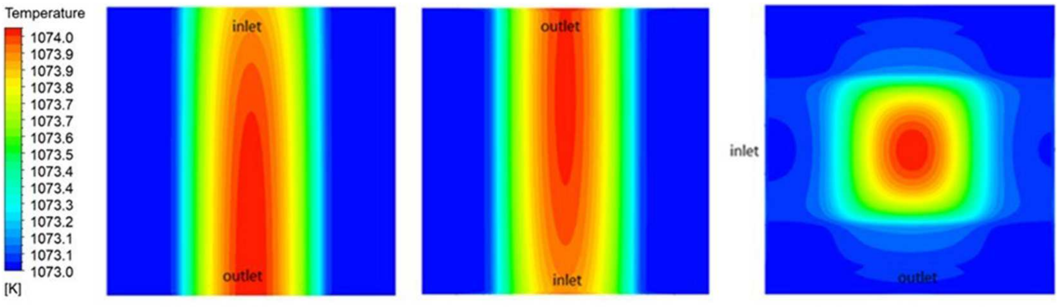

a) Parallel flow b) Counter flow c) Perpendicular flow

Figure 17. Impacts of flow configurations on temperature distribution at 1073 K and 1.3 V at the electrode-electrolyte interface: (a) parallel flow, (b) counter flow, and (c) perpendicular flow.

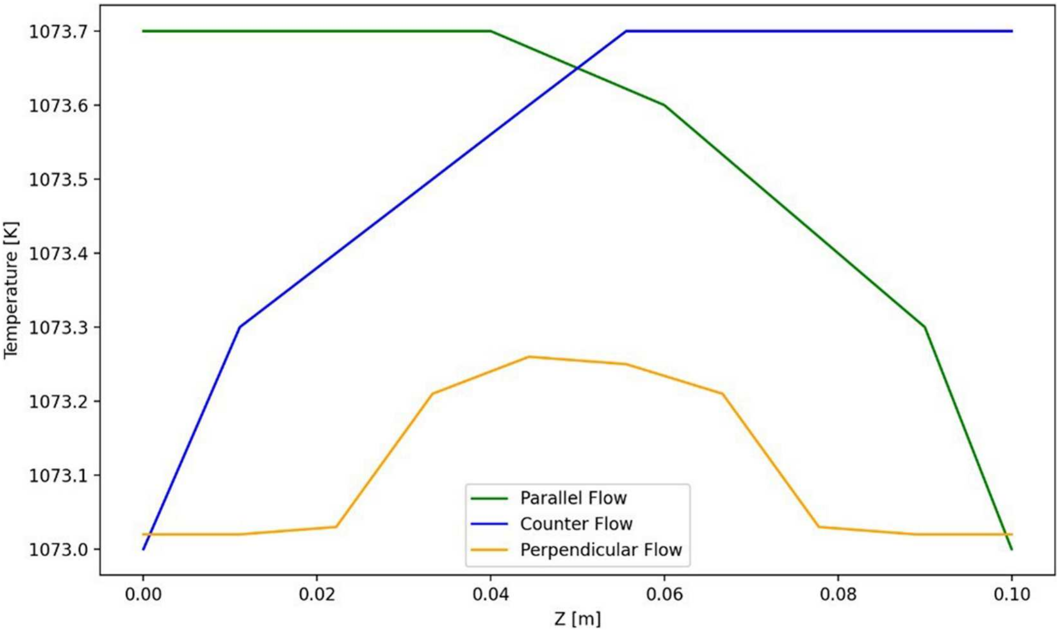

Figure 18. Temperature distribution along the flow direction at the cathode-electrolyte interface for different flow configurations.

temperature distribution in an SOEC with a parallel, counterflow, and perpendicular flow. Figure 16 shows the temperature distribution across the fuel cell components. The highest temperature is observed at the electrode–electrolyte interface, where the primary electrochemical reactions are highly exothermic (Navasa et al. 2018). The electrochemical reactions release a significant amount of heat which contributes to the localised temperature increase.

Figures 17, 18 show the impacts of the flow configurations at the electrode–electrolyte interface of the cell and along the flow direction. In both parallel and cross-flow configurations, temperatures gradually rise toward the fuel outlet, reflecting a steady and uniform temperature increase as the endothermic electrolysis reaction absorbs heat along the cell. In contrast, the counter-flow configuration shows a more pronounced temperature variation, with a localised hotspot forming at the centre of the cell. This behaviour results from the opposing directions of the fuel and oxygen streams, creating a heat exchange dynamic. As the fuel stream absorbs heat, its temperature rises, while the oxygen stream cools due to heat loss. This opposing flow creates a localised hotspot at the cell's centre, where high reaction rates and insufficient heat dissipation result in a temperature peak.

All flow configurations exhibit uneven temperature distribution, highlighting the importance of effective thermal management to minimise thermal gradients during operation. The hot spots and high-temperature regions identified in this study provide valuable insights for targeted thermal management strategies. However, as shown in Figure 18, the configurations show no significant differences in temperature distribution, resulting in no measurable impact on current density or hydrogen production. These parameters are primarily governed by factors such as electrode surface area, electrochemical kinetics, and catalyst activity, which remain unchanged across the different configurations. The minimal temperature variations can be attributed to the small size of the simulated cell and the model's operation at a thermoneutral voltage of 1.3 V. In a small cell, heat dissipates more uniformly, reducing thermal gradients and maintaining a relatively steady reaction environment. At the thermoneutral voltage, the system is theoretically in thermal equilibrium, with no significant temperature increase expected. This study primarily focuses on identifying the location of the hotspot temperature rather than its magnitude, emphasising the role of thermal management strategies in addressing localised temperature effects. In larger-scale systems, however, flow configurations may have a more pronounced effect due to increased thermal resistance, greater heat generation, and non-uniform reaction conditions. These findings highlight the importance of scaling considerations when applying thermal and flow management strategies to real-world systems.

4.1.5. Impacts of electrode porosity

The density of the TPB stands out as a crucial microstructure parameter due to its crucial role in facilitating electrochemical reactions. The TPB layer, often referred to as the active layer, consists of both ionic and electronic conductors, usually with a thickness of less than 20 micrometres, and establishes connections with the electrolyte (Zhang et al. 2021). The performance of the cell is affected by the porosity of the cathode functional layer, as TPBs rely on both porosity and composition. In this study, the porosity range of 0.1–0.9 is investigated as a theoretical framework to understand the broader impact of porosity on TBP performance. While such high porosity values may not commonly occur in practical scenarios, this theoretical exploration provides valuable insights into the influence of porosity on system behaviour and helps establish performance boundaries for guiding material design and optimisation efforts.

Figure 19 illustrates how fuel electrode porosity impacts the current density at 1.3 and 1073, 1173 and 1273 K demonstrating a linear increase in current density with higher porosity. The current density increased by 65%, 53%, and 46% when the porosity increased from 0.1 to 0.9 when the temperature was 1073, 1173, and 1273 K respectively as shown in Figure 20. Porosity affects the TPB length which affects the activation overpotential where high porosity floods the TPB with the fuel which increases the activation overpotential making the selection of porosity critical for

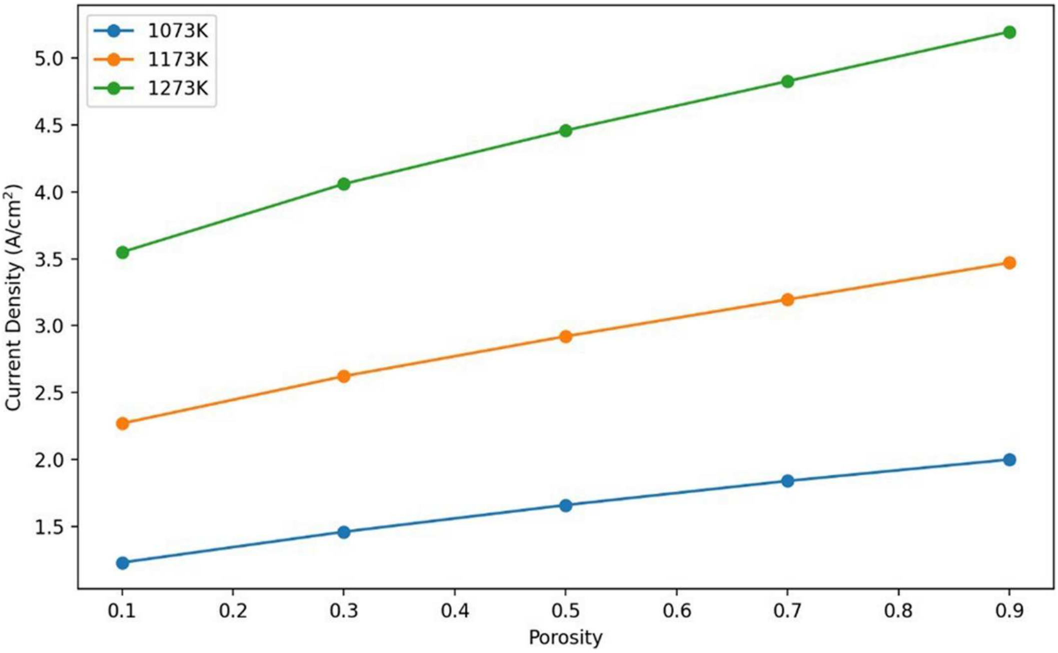

Figure 19. Current density based on fuel electrode porosity at 1.3 V and 1073, 1173 K and 1273K.

a cell (Weng et al. 2020). Sadeghifar, Djilali, and Bahrami (2014) also reported that increased porosity leads to mass transport limitations at higher current densities, which consequently results in elevated current values. This suggests that while higher porosity can improve ionic and electronic conductivity, it can also cause a reduction in the efficiency of mass transport, especially at higher current loads. This is supported by Shao et al (Shao et al. 2023) which found that the porosity level between 0.3-0.5 significantly influences both the electrolysis performance and the internal mass transport process. However, the increases in porosity lead to an increase in energy consumption (Shao et al. 2023).

Figure 21 shows the impacts of electrode porosity on hydrogen production. It is observed that the hydrogen production increases linearly with the porosity. The highest hydrogen production is obtained with 0.9 porosity at 1273 K. At higher temperatures, increased electrode porosity enhances the flow of steam to the reaction sites, improving the mobility of steam molecules and improving the efficiency of electrochemical reactions by ensuring a more uniform distribution of

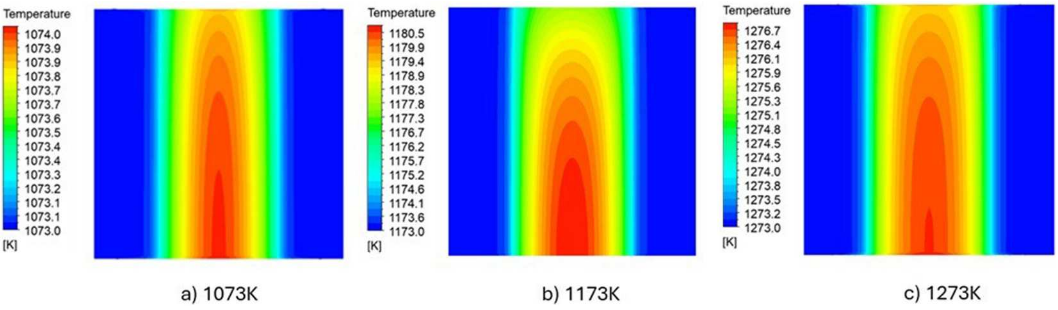

a) 1073K b) 1173K c) 1273K

Figure 20. Impacts of electrode porosity 0.9 on the temperature distribution at the electrode-electrolyte interface at 1073 K and 1.3V.

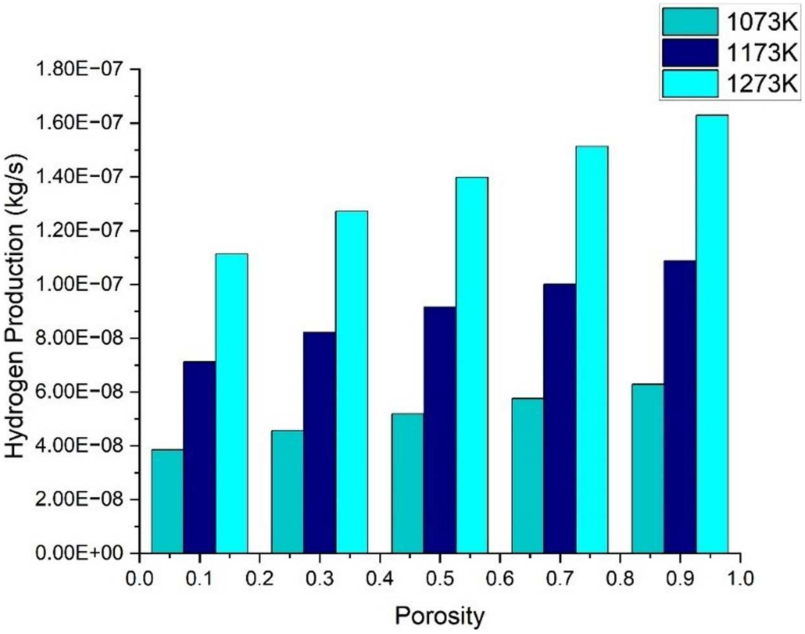

Figure 21. Hydrogen production based on fuel electrode porosity.

the reactants (Kupecki et al. 2023). This can improve the efficiency of the electrochemical reactions by ensuring that reactants are more evenly distributed across the electrode surface. However, increased porosity can reduce the mechanical strength of the electrode, necessitating a balance between robustness and steam transport efficiency (Zhang et al. 2022). Additionally, porous electrodes generally have lower thermal conductivity, which can complicate heat management and lead to localised overheating. Effective design must address these challenges to maintain both performance and durability.

4.1.6. Impacts of charge transfer coefficients

The charge transfer coefficients (CTC) are temperature-dependent parameters that vary linearly with temperature. These coefficients are considered a crucial kinetic factor for electrode reactions, as they are linked to the type and characteristics of the electrode surface and the properties of the catalyst. The CTC for a specific electrode reaction, whether anodic or cathodic, is determined by multiplying the symmetry coefficient by the number of electrons transferred during the overall electrode reaction process (Soomro et al. 2023). The symmetry coefficient ranges from 0 to 1 and is generally set to 0.5 in CFD modelling (Grondin et al. 2011; Laurencin et al. 2011; Ni, Leung, and Leung 2007) corresponding to a simple single electron exchange reaction mechanism (Bockris, Reddy, and Vijh 1972). Despite the variation in electrode reactions, the number of electrons transferred during the rate-limiting step generally does not exceed four, leading to a charge transfer coefficient (CTC) typically ranging from 0.5 to 2. In this study, the CTC values were set between 0.3 and 0.8, as reported in (Nam 2017), to examine their effects on current density, temperature distribution, and hydrogen production. Figure 22 shows the impact of CTC on the current density. It is observed that the current density rises with an increase in the charge transfer coefficient (CTC), as a higher CTC improves the efficiency of charge transfer and lowers the activation overpotential needed for the electrokinetic reactions at the electrode (Tijani, Binti Kamarudin, and Binti Mazlan 2018). Since activation overpotential contributes to the total cell voltage, a reduction in this overpotential decreases energy losses and improves efficiency, as less additional voltage is required to

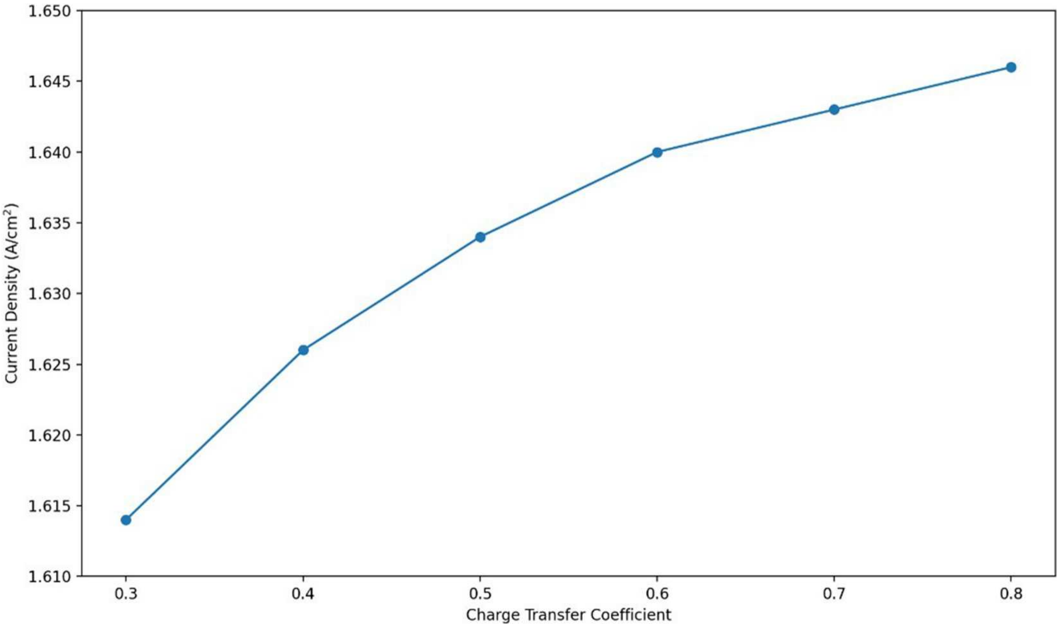

Figure 22. Effects of charge transfer coefficient on current density at 1.3 V and 1073K.

drive the reactions (Laguna-Bercero 2012). Conversely, a lower CTC results in higher activation overpotentials and increased energy losses, reducing overall efficiency.

Apart from current density, there is no significant change in hydrogen production and temperature distribution. The choice of electrode materials and their catalytic activity are directly related to the charge transfer coefficient. Materials with high catalytic activity improve charge transfer, leading to lower overpotentials and more efficient electrolysis. Therefore, selecting and developing advanced materials with high charge transfer coefficients is essential for improving SOEC performance.

4.2. RSM optimisation

The results from the parametric studies provided a fundamental understanding of how various operating conditions, such as voltage, temperature, flow configuration, porosity, and charge transfer coefficient, affect temperature distribution and current density in the SOEC. The parametric study results revealed that both operating voltage and temperature significantly influence the temperature distribution within the cell, while the steam mass fraction has a significant impact on hydrogen production. Building on these insights, optimisation studies were conducted to identify the optimal parameters that would minimise thermal gradients and hotspot formation, ultimately enhancing the performance and durability of the SOEC.

4.2.1. Analysis of variance (ANOVA)

ANOVA was used to evaluate the fit of the regression model and conduct significance tests. The model's fit was determined by the R^2 value. The R^2 value reflects how much of the variation in the response variable is explained by the model. In addition, the R^2 (adjusted) and R^2 (predicted) were calculated to assess the model's predictive ability and accuracy after adjusting for precision where the prediction error sum of squares measures how well the model predicts new data. The R^2 (appropriate), R^2 (predicted), and R^2 (adjusted) values reflect the model's overall fit, its ability to predict new data, and its accuracy after adjusting for precision, respectively (Chen et al.

Table 8. Summary of statistical metrics and formulas.

Term	Formula	Limit
Model Mean of Square	Total Sum of Square Model / Degree of Freedom Model	
Error Mean Square	Total Sum of Square Error / Degree of Freedom Residual	
R^2	1-[Total Sum of Square Error/(Total Sum of Square Model + Total Sum of Square Error)]	Near or close to 1
R^2 (adjusted)	1-{[Total Sum of Square Error/Degree of Freedom Error]/[(Total Sum of Square Model + Total Sum of Square Error)/ (Degree of Freedom Model + Degree of Freedom Error)}	Near or close to 1
R^2 (predicted)	1 − (Prediction Error Sum of Square/ Total Sum of Square)	The difference between R^2 (adjusted) and R^2 (predicted) should be less than 0.2
F-value	Model Mean Square /Error Mean Square	

2023). The R^2 value for this model is 1, indicating an excellent fit to the simulation data. An R^2 value above 0.75 typically suggests good and satisfactory model performance. The adjusted R^2 value of 0.99, while slightly lower than R^2, is close to 1 and indicates an acceptable level of goodness-of-fit The significance of each term in the regression model is assessed using the F and *P* values. The *F*-value is calculated as the ratio of the mean square of the factor to the mean square of the error, while the *P*-value represents the probability associated with the *F*-test. Typically, the most significant terms in the model correspond to the minimum *P*-value and the maximum *F*-value. For a model to be considered a good predictor, the *F*-value should be greater than 4 (Raeisian et al. 2019). The formula to calculate the statistical term (Breig and Luti 2021) was tabulated in Table 8.

As shown in Table 9, the results of the analysis of variance (ANOVA) confirm the statistical significance of the model's terms, as indicated by the *P*-values. A *P*-value less than or equal to 0.05 indicates that the term is statistically significant, while a *P*-value greater than 0.05 suggests a negligible effect. In this case, the *F*-value of 32,898 suggests that most of the variations in the response can be explained by the regression equation, indicating that the model is highly significant. With a *P*-value below 0.05, the model is statistically significant. The ANOVA results show that temperature and voltage have the greatest impact on hotspot temperature, followed by steam mass fraction.

Table 9. Analysis Variance (ANOVA) for response quadratic model.

Source	Degree Freedom (DF)	Adjusted Sum of Square	Adjusted Mean Square	*F*-value	*P*-value	Remarks
Model	9	42,225.5	4691.7	32,898.15	0.000	
Linear	3	42,155.7	14,051.9	98,531.22	0.000	
T	1	41,922.6	41,922.6	293,959.00	0.000	Significant
V	1	232.6	232.6	1630.72	0.000	Significant
SMF	1	0.6	0.6	3.94	0.075	Significant
Square	3	59.5	59.5	128.98	0.000	
T*T	1	4.2	4.2	29.5	0.000	Significant
V*V	1	59.2	59.2	414.91	0.000	Significant
SMF*SMF	1	4.2	4.2	29.50	0.000	Significant
2-way Interaction	3	10.4	3.5	24.25	0.000	
T*V	1	10.1	10.1	71.00	0.000	Significant
T*SMF	1	0.1	0.1	0.88	0.371	Not significant
V*SMF	1	0.1	0.1	0.88	0.371	Not significant
Error	10	1.4	0.1			
Lack-of-fit	5	1.4	0.3			
Pure Error	5	0.0	0.0			
Total	19	42,227.0				
R^2	1.0	R^2_{adj}	0.99			

4.2.2. Regression equation models

Regression equation models are vital in statistical analysis as they represent and explain the relationship between a dependent variable and one or more independent variables. By examining these relationships, regression models enable the prediction or explanation of changes in the dependent variable based on variations in the independent variables. The quadratic regression models for the corresponding output responses are expressed by Equation (8).

$$\begin{aligned}\mathrm{HST} = {} & 802.8 + 0.3299\mathrm{T} - 633.4\mathrm{V} - 101.0\mathrm{SMF} + 0.000164\mathrm{T}^2 + 153.41\mathrm{V}^2 + 40.91\mathrm{SMF}^2 \\ & + 0.2250\ \mathrm{T}{*}\mathrm{V} + 0.0250\mathrm{T}{*}\mathrm{SMF} + 12.5\mathrm{V}{*}\mathrm{SMF}\end{aligned} \tag{8}$$

where T is the operating temperature, V is the operating voltage and SMF is the steam mass fraction.

4.2.3. Response surface analysis

Figure 24 illustrates the interaction between the independent variables and their combined effects on hotspot temperature through surface contours. In this plot, the steam mass fraction is maintained at its central value within the specified operating range, allowing for a focused analysis of the interaction between the two factors being examined, while the impact of the other factor is held constant. As shown in Figures 23 and 24, the hotspot temperature rises with increasing operating temperature and voltage. The highest hotspot temperature was observed at the highest operating conditions.

4.2.4. Optimisation of designing parameters

Following the simultaneous optimisation of the decision variables, the optimal independent variables were determined using the RSM optimiser module in MINITAB. Each result was assigned a unitless desirability value ranging from 0 to 1, where 1 signifies the ideal optimised response and 0 indicates an undesirable outcome. The optimisation aimed to minimise the hot spot temperature of the SOEC during operation. The results from the RSM optimiser are shown in Figure 25

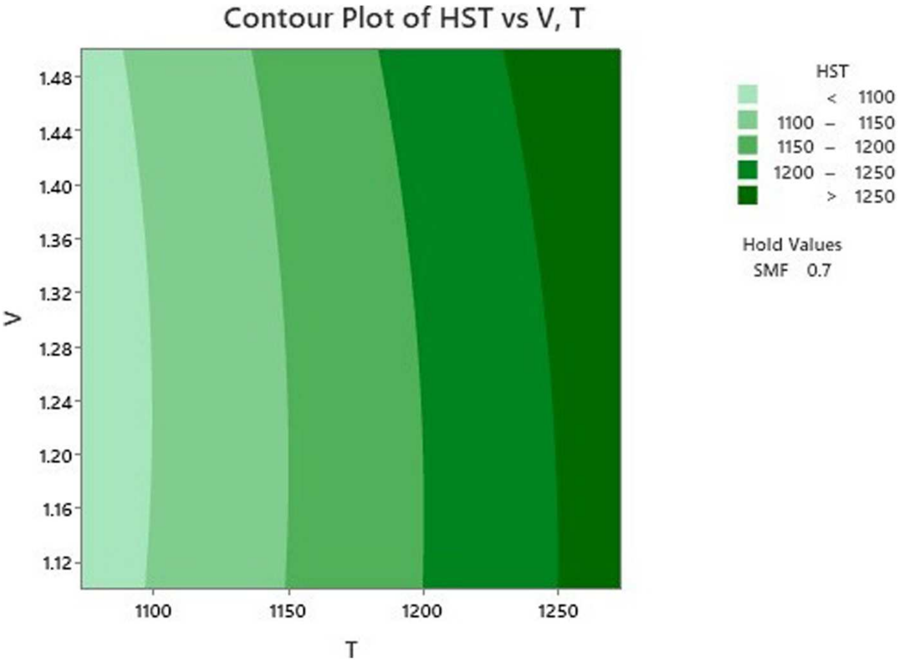

Figure 23. Effects of operating temperature (T) and operating voltage (V) on hot spot temperature (HST).

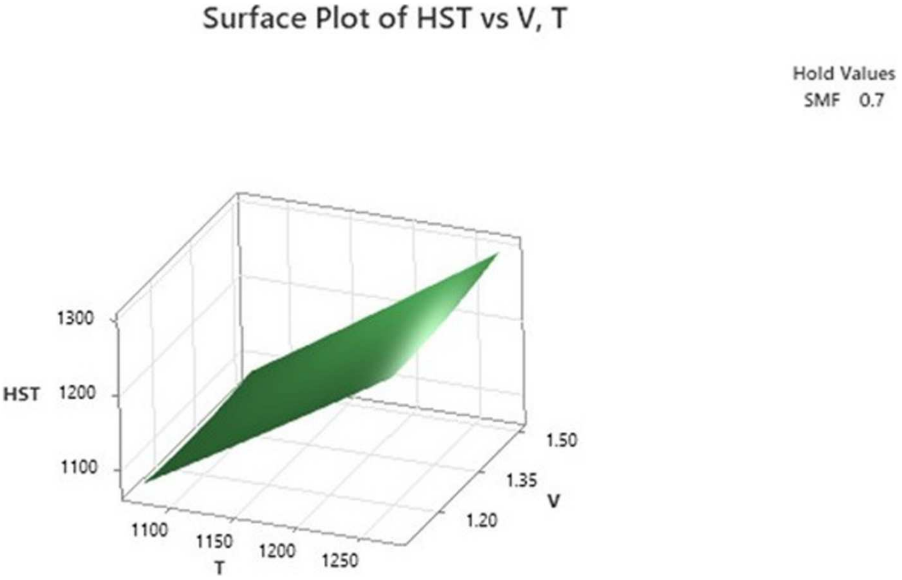

Figure 24. Surface plot of Hot Spot Temperature (HST) vs Operating Voltage (V) and Operating Temperature (T).

below. The optimal values for the operating temperature (T), operating voltage (V), and steam mass fraction (SMF) are 1073 K, 1.5 V, and 0.9, respectively, resulting in a predicted hot spot temperature (HST) of 1085 K at the electrode–electrolyte interface. Operating at 1073 K offers a favourable balance between efficiency and material stability allowing for better thermal management through

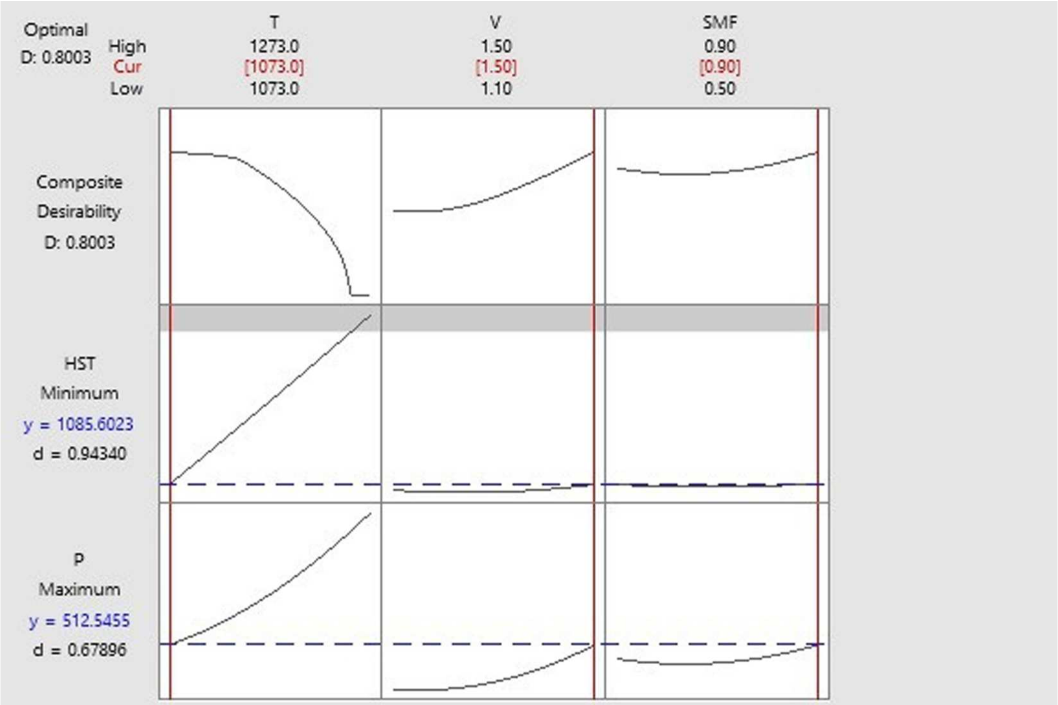

Figure 25. RSM Optimiser.

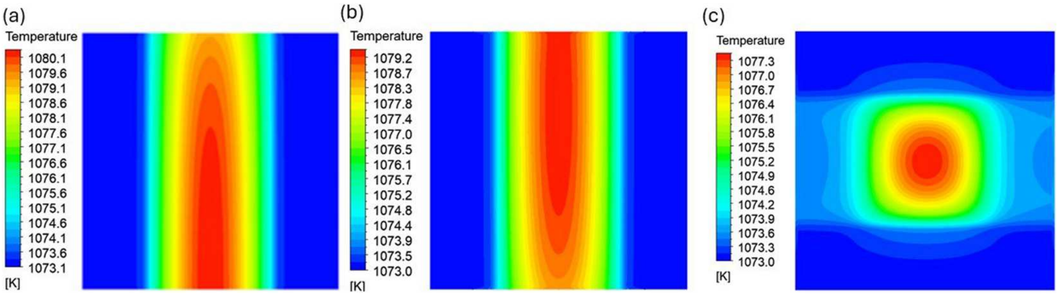

Figure 26. (a) Parallel flow (b) Crossflow (c) Perpendicular flow.

advanced heat exchange systems and insulation that stabilise cell temperature while potentially leveraging waste heat from other industrial processes to reduce operating costs.

4.2.5. Validation of optimised parameters

CFD simulations were conducted using the optimised parameters, yielding a hot spot temperature (HST) of 1080 K. This result shows a 0.5% deviation from the predicted HST of 1086 K from the RSM model. The simulations were repeated for three different flow configurations, as shown in Figure 26. The HST values for parallel flow, cross-flow, and perpendicular flow were 1080 K, 1079 K, and 1077 K, respectively, with the perpendicular flow configuration resulting in the lowest hot spot temperature.

This study examines the impacts and optimisation of operating parameters on temperature distribution and cell performance, relying on specific assumptions about material properties and steady-state conditions. While these assumptions simplify the analysis, they may not fully capture the complexities of real-world SOECs, potentially leading to discrepancies between simulated and actual performance. Additionally, the focus on steady-state conditions excludes dynamic behaviours such as varying loads, start-up, and shut-down cycles.

Future research will address these limitations by extending the mathematical model and computational fluid dynamics (CFD) framework to incorporate time-dependent governing equations and boundary conditions. This will enable the simulation of transient phenomena, such as the response of temperature distribution to sudden changes in operating conditions, and provide a deeper understanding of start-stop processes and their effects on cell lifetime and durability. A comprehensive investigation of material properties, fluid dynamics, and heat transfer will also be critical for enhancing the thermal performance and design of SOECs.

Even though evaluating cell performance at the individual cell level is crucial for design, operation, control, and optimisation, ensuring effective thermal management for commercially viable SOECs requires expanding considerations to stack and system levels. This broader approach enables an understanding of cell-to-cell thermal interactions and variations in thermochemical performance across cell units. Utilising modelling techniques allows for the exploration of stack behaviour in practical applications, aiding in the development of optimal stack designs and operational strategies.

5. Conclusion

This study demonstrates that optimising operating parameters such as voltage, temperature, and steam mass fraction using Response Surface Methodology (RSM) significantly improves Solid Oxide Electrolyser Cell (SOEC) performance. The parametric analysis revealed that increasing voltage from 1.1 to 1.5 V raises current density from 0.75 A/cm^2 to 2.5 A/cm^2, with proportional increases in hydrogen production and thermal gradients, reaching up to 15 K at higher temperatures. The optimal operating conditions, 1073, 1.5 V, and a steam mass fraction of 0.9, minimised hotspot temperature to 1086 K, as confirmed by simulations.

These findings establish a foundation for minimising thermal gradients, reducing material degradation, and extending the lifespan of Solid Oxide Electrolyser Cells (SOECs), thereby improving their efficiency and durability. By identifying optimal operating conditions, including voltage, temperature, and steam mass fraction, this study provides practical insights that enhance the performance and reliability of SOECs. These advancements directly support hydrogen production, making SOECs more viable for industrial-scale applications and contributing to the development of sustainable energy solutions.

The study highlights the importance of advanced thermal management strategies to ensure consistent temperature distribution and long-term cell stability. Proposed solutions include optimised convective cooling, integration of heat pipes or phase change materials (PCM), and self-adaptive methods such as thermochemical energy storage (TES). These approaches, combined with optimised operational parameters, enable scalable and sustainable green hydrogen production, supporting renewable energy integration and global decarbonisation efforts.

Disclosure statement

No potential conflict of interest was reported by the authors.

Data availability statement

The data supporting this study are available upon request.

References

Aguiar, P., C. S. Adjiman, and N. P. Brandon. 2004. “Anode-Supported Intermediate Temperature Direct Internal Reforming Solid Oxide Fuel Cell. I: Model-Based Steady-State Performance.” *Journal of Power Sources* 138:120–136. https://doi.org/10.1016/j.jpowsour.2004.06.040.

ANSYS. 2023. *ANSYS Fluent Theory Guide*. Ansys Inc.

Arvay, A., A. Ahmed, X. H. Peng, and A. M. Kannan. 2012. “Convergence Criteria Establishment for 3D Simulation of Proton Exchange Membrane Fuel Cell.” *International Journal of Hydrogen Energy* 37:2482–2489. https://doi.org/10.1016/j.ijhydene.2011.11.005.

Barari, F., R. Morgan, and P. Barnard. 2014. “A Design of Experiments (DOE) Approach to Optimise Temperature Measurement Accuracy in Solid Oxide Fuel Cell (SOFC).” *Journal of Physics: Conference Series* 547:012004. https://doi.org/10.1088/1742-6596/547/1/012004.

Barelli, L., G. Bidini, and G. Cinti. 2018. “Steam as Sweep Gas in SOE Oxygen Electrode.” *Journal of Energy Storage* 20:190–195. https://doi.org/10.1016/j.est.2018.09.009.

Benedetti, B., V. Caponigro, and F. Ardini. 2022. “Experimental Design Step by Step: A Practical Guide for Beginners.” *Critical Reviews in Analytical Chemistry* 52:1015–1028. https://doi.org/10.1080/10408347.2020.1848517.

Bockris, J. O., A. K. N. Reddy, and A. K. Vijh. 1972. “Modern Electrochemistry.” *Journal of The Electrochemical Society* 119:136C. https://doi.org/10.1149/1.2404214.

Breig, S. J. M., and K. J. K. Luti. 2021. “Response Surface Methodology: A Review on Its Applications and Challenges in Microbial Cultures.” *Materials Today: Proceedings* 42:2277–2284. https://doi.org/10.1016/j.matpr.2020.12.316.

Cai, Q., E. Luna-Ortiz, C. S. Adjiman, and N. P. Brandon. 2010. “The Effects of Operating Conditions on the Performance of a Solid Oxide Steam Electrolyser: A Model-Based Study.” *Fuel Cells* 10:1114–1128. https://doi.org/10.1002/fuce.200900211.

Chen, H., J. Wang, and X. Xu. 2023. “Parametric Study of Operating Conditions on Performances of a Solid Oxide Electrolysis Cell.” *Journal of Thermal Science* 32:1973–1988. https://doi.org/10.1007/s11630-023-1772-4.

Chen, Z., W. Zuo, K. Zhou, Q. Li, Y. Huang, and J. E. 2023. “Multi-objective Optimization of Proton Exchange Membrane Fuel Cells by RSM and NSGA-II.” *Energy Conversion and Management* 277:116691. https://doi.org/10.1016/j.enconman.2023.116691.

Cui, Y., Z. Wang, L. Yang, J. Li, G. Chang, L. Song, and G. Yue. 2024. "Multi-objective Optimization Design of the Solid Oxide Fuel Cells Using Response Surface Methodology and Genetic Algorithm." *Applied Thermal Engineering* 242:122503. https://doi.org/10.1016/j.applthermaleng.2024.122503.

Cui, T., G. Xiao, H. Yan, Y. Zhang, and J. Q. Wang. 2023. "Numerical Simulation and Analysis of the Thermal Stresses of a Planar Solid Oxide Electrolysis Cell." *International Journal of Green Energy* 20:432–444. https://doi.org/10.1080/15435075.2022.2065881.

Faghri, A., and Z. Guo. 2005. "Challenges and Opportunities of Thermal Management Issues Related to Fuel Cell Technology and Modeling." *International Journal of Heat and Mass Transfer* 48:3891–3920. https://doi.org/10.1016/j.ijheatmasstransfer.2005.04.014.

Fang, Z., Z. Liu, S. Zhang, Z. Yang, and X. Huang. 2024. "Performance Evaluation and Multi-Objective Optimization of a Solar-Thermal-Assisted Energy System: Supercritical CO2 Brayton Cycle and Solid Oxide Electrolysis/Fuel Cells." *Energy Conversion and Management* 308:118404. https://doi.org/10.1016/j.enconman.2024.118404.

Ferrero, D., A. Lanzini, P. Leone, and M. Santarelli. 2017. "DOE Methodologies for Analysis of Large SOFC Systems." *CISM International Centre for Mechanical Sciences, Courses and Lectures*, 574:265–289. https://doi.org/10.1007/978-3-319-46146-5_7.

Fu, Q., Z. Li, W. Wei, F. Liu, X. Xu, and Z. Liu. 2021. "Performance Enhancement of Planar Solid Oxide Fuel Cell Using a Novel Interconnector Design." *International Journal of Hydrogen Energy* 46:21634–21656. https://doi.org/10.1016/j.ijhydene.2021.04.001.

Gaikwad, P. S., K. Mondal, Y. K. Shin, A. C. T. van Duin, and G. Pawar. 2023. "Enhancing the Faradaic Efficiency of Solid Oxide Electrolysis Cells: Progress and Perspective." *NPJ Computational Materials* 9: 149. https://doi.org/10.1038/s41524-023-01044-1.

Ghorbani, B., and K. Vijayaraghavan. 2018. "3D and Simplified Pseudo-2D Modeling of Single Cell of a High Temperature Solid Oxide Fuel Cell to be Used for Online Control Strategies." *International Journal of Hydrogen Energy* 43:9733–9748. https://doi.org/10.1016/j.ijhydene.2018.03.211.

Graves, C., S. D. Ebbesen, M. Mogensen, and K. S. Lackner. 2011. "Sustainable Hydrocarbon Fuels by Recycling CO2 and H2O with Renewable or Nuclear Energy." *Renewable and Sustainable Energy Reviews* 15: 1–23.

Grondin, D., J. Deseure, A. Brisse, M. Zahid, and P. Ozil. 2010. "Simulation of a High Temperature Electrolyzer." *Journal of Applied Electrochemistry* 40:933–941. https://doi.org/10.1007/s10800-009-0030-0.

Grondin, D., J. Deseure, P. Ozil, J. P. Chabriat, B. Grondin-Perez, and A. Brisse. 2011. "Computing Approach of Cathodic Process Within Solid Oxide Electrolysis Cell: Experiments and Continuum Model Validation." *Journal of Power Sources* 196:9561–9567. https://doi.org/10.1016/j.jpowsour.2011.07.033.

Hauch, A., and P. Blennow. 2023. "Solid Oxide Electrolysis Cells – Interplay Between Operating Conditions, Fuel Electrode Overpotential and Degradation." *Solid State Ionics* 391:116127. https://doi.org/10.1016/j.ssi.2022.116127.

Hawkes, G., J. O'Brien, C. Stoots, and B. Hawkes. 2009. "3D CFD Model of a Multi-Cell High-Temperature Electrolysis Stack." *International Journal of Hydrogen Energy* 34:4189–4197. https://doi.org/10.1016/j.ijhydene.2008.11.068.

Kamkeng, A. D. N., and M. Wang. 2022. "Long-term Performance Prediction of Solid Oxide Electrolysis Cell (SOEC) for CO_2/H_2O co-Electrolysis Considering Structural Degradation Through Modelling and Simulation." *Chemical Engineering Journal* 429:132158. https://doi.org/10.1016/j.cej.2021.132158.

Kang, C., P. Huaiwu, Z. Junfeng, X. Xinxin, Z. Shengchen, R. Jingxin, L. Biao, and W. Yueshe. 2022. "Analysis of Performance Optimization of High-Temperature Solid Oxide Electrolytic Cell Based on the Coupling of Flow, Heat, and Mass Transfer and Electrochemistry." *Energy Science & Engineering* 10:3918–3927. https://doi.org/10.1002/ese3.1255.

Kim, H., M. Park, and K. S. Lee. 2013. "One-dimensional Dynamic Modeling of a High-Pressure Water Electrolysis System for Hydrogen Production." *International Journal of Hydrogen Energy* 38:2596–2609. https://doi.org/10.1016/j.ijhydene.2012.12.006.

Koh, J. H., D. J. Yoon, and C. H. Oh. 2010. "Simple Electrolyzer Model Development for High-Temperature Electrolysis System Analysis Using Solid Oxide Electrolysis Cell." *Journal of Nuclear Science and Technology* 47:599–607. https://doi.org/10.3327/jnst.47.599.

Kupecki, J., A. Niemczyk, S. Jagielski, R. Kluczowski, M. Kosiorek, and K. Machaj. 2023. "Boosting Solid Oxide Electrolyzer Performance by Fine Tuning the Microstructure of Electrodes – Preliminary Study." *International Journal of Hydrogen Energy* 48:26436–26445. https://doi.org/10.1016/j.ijhydene.2022.04.074.

Laguna-Bercero, M. A. 2012. "Recent Advances in High Temperature Electrolysis Using Solid Oxide Fuel Cells: A Review." *Journal of Power Sources* 203:4–16. https://doi.org/10.1016/j.jpowsour.2011.12.019.

Lang, M., S. Raab, M. S. Lemcke, C. Bohn, and M. Pysik. 2020. "Long-Term Behavior of a Solid Oxide Electrolyzer (SOEC) Stack." *Fuel Cells* 20:690–700. https://doi.org/10.1002/fuce.201900245.

Laurencin, J., D. Kane, G. Delette, J. Deseure, and F. Lefebvre-Joud. 2011. "Modelling of Solid Oxide Steam Electrolyser: Impact of the Operating Conditions on Hydrogen Production." *Journal of Power Sources* 196:2080–2093. https://doi.org/10.1016/j.jpowsour.2010.09.054.

Le Liu, T., C. Wang, S.-J. Hao, Z.-Q. Fu, B. A. Peppley, Z.-M. Mao, J.-L. Wang, and Z.-Q. Mao. 2016. "Evaluation of Polarization and Hydrogen Production Efficiency of Solid Oxide Electrolysis Stack with La0.6Sr0.4Co0.2Fe0.8O3 −δ- Ce0.9Gd0.1O1.95 Oxygen Electrode." *International Journal of Hydrogen Energy* 41:15970–15978. https://doi.org/10.1016/j.ijhydene.2016.04.243.

Lu, B., Z. Zhang, Z. Zhang, C. Zhang, L. Zhu, and Z. Huang. 2024. "Control Strategy of Solid Oxide Electrolysis Cell Operating Temperature Under Real Fluctuating Renewable Power." *Energy Conversion and Management* 299:117852. https://doi.org/10.1016/j.enconman.2023.117852.

Mahmood, A., S. Bano, J. H. Yu, and K. H. Lee. 2015. "Effect of Operating Conditions on the Performance of Solid Electrolyte Membrane Reactor for Steam and CO2 Electrolysis." *Journal of Membrane Science* 473:8–15. https://doi.org/10.1016/j.memsci.2014.09.002.

Menon, V., V. M. Janardhanan, and O. Deutschmann. 2014. "A Mathematical Model to Analyze Solid Oxide Electrolyzer Cells (SOECs) for Hydrogen Production." *Chemical Engineering Science* 110:83–93. https://doi.org/10.1016/j.ces.2013.10.025.

Min, G., Y. J. Park, S. Choi, and J. Hong. 2021. "Sensitivity Analysis of a Solid Oxide co-Electrolysis Cell System with Respect to Its Key Operating Parameters and Optimization with its Performance map." *Energy Conversion and Management* 249:114848. https://doi.org/10.1016/j.enconman.2021.114848.

Mojaver, P., S. Khalilarya, and A. Chitsaz. 2019. "Multi-objective Optimization Using Response Surface Methodology and Exergy Analysis of a Novel Integrated Biomass Gasification, Solid Oxide Fuel Cell and High-Temperature Sodium Heat Pipe System." *Applied Thermal Engineering* 156:627–639. https://doi.org/10.1016/j.applthermaleng.2019.04.104.

Nam, J. H. 2017. "Electrochemical Effectiveness Factors for Butler-Volmer Reaction Kinetics in Active Electrode Layers of Solid Oxide Fuel Cells." *Journal of Electrochemical Science and Technology* 8(4): 344–355. https://doi.org/10.5229/JECST.2017.8.4.344.

Namwong, L., S. Authayanun, D. Saebea, Y. Patcharavorachot, and A. Arpornwichanop. 2016. "Modeling and Optimization of Proton-Conducting Solid Oxide Electrolysis Cell: Conversion of CO2 Into Value-Added Products." *Journal of Power Sources* 331:515–526. https://doi.org/10.1016/j.jpowsour.2016.09.042.

Navasa, M., C. Graves, C. Chatzichristodoulou, T. Løye Skafte, B. Sundén, and H. Lund Frandsen. 2018. "A Three Dimensional Multiphysics Model of a Solid Oxide Electrochemical Cell: A Tool for Understanding Degradation." *International Journal of Hydrogen Energy* 43:11913–11931. https://doi.org/10.1016/j.ijhydene.2018.04.164.

Navasa, M., J. Yuan, and B. Sundén. 2015. "Computational Fluid Dynamics Approach for Performance Evaluation of a Solid Oxide Electrolysis Cell for Hydrogen Production." *Applied Energy* 137:867–876. https://doi.org/10.1016/j.apenergy.2014.04.104.

Nguyen, H. L., Y. Kim, J. Park, and S. Yu. 2023. "Operating Strategy Optimization by Response Surface Analysis for Durable Operation of a Heavy-Duty Fuel Cell Truck." *Energy Conversion and Management* 291:117295. https://doi.org/10.1016/j.enconman.2023.117295.

Ni, M. 2009. "Computational Fluid Dynamics Modeling of a Solid Oxide Electrolyzer Cell for Hydrogen Production." *International Journal of Hydrogen Energy* 34:7795–7806. https://doi.org/10.1016/j.ijhydene.2009.07.080.

Ni, M., M. K. H. Leung, and D. Y. C. Leung. 2007. "Parametric Study of Solid Oxide Steam Electrolyzer for Hydrogen Production." *International Journal of Hydrogen Energy* 32:2305–2313. https://doi.org/10.1016/j.ijhydene.2007.03.001.

O'Brien, J. E., C. M. Stoots, and J. S. Herring. 2010. *High Temperature Electrolysis for Hydrogen Production from Nuclear Energy – Technology Summary*. Idaho: Idaho Natl. Lab. Idaho Falls.

Petipas, F., A. Brisse, and C. Bouallou. 2017. "Thermal Management of Solid Oxide Electrolysis Cell Systems Through air Flow Regulation." *Chemical Engineering Transactions* 61: 1069–1074. https://doi.org/10.3303/CET1761176.

Raeisian, L., H. Niazmand, E. Ebrahimnia-Bajestan, and P. Werle. 2019. "Thermal Management of a Distribution Transformer: An Optimization Study of the Cooling System Using CFD and Response Surface Methodology." *International Journal of Electrical Power & Energy Systems* 104:443–455. https://doi.org/10.1016/j.ijepes.2018.07.043.

Reytier, M., S. Di Iorio, A. Chatroux, M. Petitjean, J. Cren, M. De Saint Jean, J. Aicart, and J. Mougin. 2015. "Stack Performances in High Temperature Steam Electrolysis and co-Electrolysis." *International Journal of Hydrogen Energy* 40:11370–11377. https://doi.org/10.1016/j.ijhydene.2015.04.085.

Roy, D., S. Samanta, and S. Ghosh. 2020. "Performance Optimization Through Response Surface Methodology of an Integrated Biomass Gasification Based Combined Heat and Power Plant Employing Solid Oxide Fuel Cell and Externally Fired gas Turbine." *Energy Conversion and Management* 222:113182. https://doi.org/10.1016/j.enconman.2020.113182.

Sadeghifar, H., N. Djilali, and M. Bahrami. 2014. "Effect of Polytetrafluoroethylene (PTFE) and Micro Porous Layer (MPL) on Thermal Conductivity of Fuel Cell gas Diffusion Layers: Modeling and Experiments." *Journal of Power Sources* 248:632–641. https://doi.org/10.1016/j.jpowsour.2013.09.136.

Sahu, J. N., J. Acharya, and B. C. Meikap. 2009. "Response Surface Modeling and Optimization of Chromium(VI) Removal from Aqueous Solution Using Tamarind Wood Activated Carbon in Batch Process." *Journal of Hazardous Materials* 172:818–825. https://doi.org/10.1016/j.jhazmat.2009.07.075.

Samavati, M., M. Santarelli, A. Martin, and V. Nemanova. 2017. "Thermodynamic and Economy Analysis of Solid Oxide Electrolyser System for Syngas Production." *Energy* 122:37–49. https://doi.org/10.1016/j.energy.2017.01.067.

Schefold, J., and H. Pöpke. 2022. "(Invited) Durability of Electrolyte Supported Solid Oxide Cells for Steam Electrolysis: Results from Cell Testing in the 20,000 h to 50,000 Hours Range." *ECS Meeting Abstracts* MA2022-01:1738–1738. https://doi.org/10.1149/ma2022-01391738mtgabs.

Shao, Y., Y. Li, Z. Fu, J. Li, and Q. Zhu. 2023. "Numerical Investigation on the Performance of IT-SOEC with Double-Layer Composite Electrode." *Energies* 16:2525. https://doi.org/10.3390/en16062525.

Sharafinia, S., A. Farrokhnia, and E. Ghasemian Lemraski. 2022. "Optimized Safranin Adsorption Onto Poly(Vinylidene Fluoride)-Based Nanofiber Via Response Surface Methodology." *Materials Chemistry and Physics* 276:125407. https://doi.org/10.1016/j.matchemphys.2021.125407.

Shimada, H., T. Yamaguchi, H. Kishimoto, H. Sumi, Y. Yamaguchi, K. Nomura, and Y. Fujishiro. 2019. "Nanocomposite Electrodes for High Current Density Over 3 A cm−2 in Solid Oxide Electrolysis Cells." *Nature Communications* 10 (1): 5432. https://doi.org/10.1038/s41467-019-13426-5.

Sofiah, A. G. N., J. Pasupuleti, M. Samykano, A. K. Pandey, R. K. Rajamony, N. F. Sulaiman, and Z. A. Che Ramli. 2024. "A Class of Promising Fuel Cell Performance: International Status on the Application of Nanofluids for Thermal Management Systems." *Materials Today Sustainability* 26:100709. https://doi.org/10.1016/j.mtsust.2024.100709.

Soomro, I. A., F. H. Memon, W. Mughal, M. A. Khan, W. Ali, Y. Liu, K. H. Choi, and K. H. Thebo. 2023. "Influence of Operating and Electrochemical Parameters on PEMFC Performance: A Simulation Study." *Membranes* 13:259. https://doi.org/10.3390/membranes13030259.

Sriram Srinivas, J. T., S. R. Dhanushkodi, R. K. Chidambaram, D. Skrzyniowska, and A. Korzen. 2023. "Benchmarking Electrolytes for the Solid Oxide Electrolyzer Using a Finite Element Model." *Energies* 16 (18): 6419. https://doi.org/10.3390/en16186419.

Tijani, A. S., N. A. Binti Kamarudin, and F. A. Binti Mazlan. 2018. "Investigation of the Effect of Charge Transfer Coefficient (CTC) on the Operating Voltage of Polymer Electrolyte Membrane (PEM) Electrolyzer." *International Journal of Hydrogen Energy* 43:9119–9132. https://doi.org/10.1016/j.ijhydene.2018.03.111.

Tikiz, I., and I. Taymaz. 2016. "An Experimental Investigation of Solid Oxide Fuel Cell Performance at Variable Operating Conditions." *Thermal Science* 20 (5): 1421–1433. https://doi.org/10.2298/TSCI130617019 T.

Udagawa, J., P. Aguiar, and N. P. Brandon. 2007. "Hydrogen Production Through Steam Electrolysis: Model-Based Steady State Performance of a Cathode-Supported Intermediate Temperature Solid Oxide Electrolysis Cell." *Journal of Power Sources* 166:127–136. https://doi.org/10.1016/j.jpowsour.2006.12.081.

UK Hydrogen Strategy. 2021. *Chemistry & Industry* 85:17. https://doi.org/10.1002/cind.859_6.x.

Wang, L., M. Pérez-Fortes, H. Madi, S. Diethelm, J. Van herle, and F. Maréchal. 2018. "Optimal Design of Solid-Oxide Electrolyzer Based Power-to-Methane Systems: A Comprehensive Comparison Between Steam Electrolysis and co-Electrolysis." *Applied Energy* 211:1060–1079. https://doi.org/10.1016/j.apenergy.2017.11.050.

Wang, H., L. Xiao, Y. Liu, X. Zhang, R. Zhou, F. Liu, and J. Yuan. 2023. "Performance and Thermal Stress Evaluation of Full-Scale SOEC Stack Using Multi-Physics Modeling Method." *Energies* 16:7720. https://doi.org/10.3390/en16237720.

Weng, F. B., M. M. Dlamini, G. bin Jung, and C. X. Lian. 2020. "Analyses of Reversible Solid Oxide Cells Porosity Effects on Temperature Reduction." *International Journal of Hydrogen Energy* 45:12170–12184. https://doi.org/10.1016/j.ijhydene.2020.02.157.

Xu, Y., S. Cai, B. Chi, and Z. Tu. 2023. "Technological Limitations and Recent Developments in a Solid Oxide Electrolyzer Cell: A Review." *International Journal of Hydrogen Energy* 50:548–591. https://doi.org/10.1016/j.ijhydene.2023.08.314.

Xu, Z., N. Ren, M. Tang, X. Zhang, F. Wang, and G. Li. 2019. "Numerical Investigations for a Solid Oxide Electrolyte Cell Stack." *International Journal of Hydrogen Energy* 44 (38): 20997–21009. https://doi.org/10.1016/j.ijhydene.2019.04.141.

Xu, Z., X. Zhang, G. Li, G. Xiao, and J. Q. Wang. 2017. "Comparative Performance Investigation of Different gas Flow Configurations for a Planar Solid Oxide Electrolyzer Cell." *International Journal of Hydrogen Energy* 42:10785–10801. https://doi.org/10.1016/j.ijhydene.2017.02.097.

Yan, Z., A. He, S. Hara, and N. Shikazono. 2019. "Modeling of Solid Oxide Fuel Cell (SOFC) Electrodes from Fabrication to Operation: Correlations Between Microstructures and Electrochemical Performances." *Energy Conversion and Management* 190:1–13. https://doi.org/10.1016/j.enconman.2019.04.002.

Zhang, X., M. Espinoza, T. Li, and M. Andersson. 2021. "Parametric Study for Electrode Microstructure Influence on SOFC Performance." *International Journal of Hydrogen Energy* 46:37440–37459. https://doi.org/10.1016/j.ijhydene.2021.09.057.

Zhang, X., J. E. O'Brien, G. Tao, C. Zhou, and G. K. Housley. 2015. "Experimental Design, Operation, and Results of a 4 kW High Temperature Steam Electrolysis Experiment." *Journal of Power Sources* 297:90–97. https://doi.org/10.1016/j.jpowsour.2015.07.098.

Zhang, M., E. Wang, J. Mao, H. Wang, M. Ouyang, and H. Hu. 2022. "Performance Analysis of a Metal-Supported Intermediate-Temperature Solid Oxide Electrolysis Cell." *Frontiers in Energy Research* 10: 888787. https://doi.org/10.3389/fenrg.2022.888787.

Zhao, J., Z. Lin, and M. Zhou. 2022. "Three-Dimensional Modeling and Performance Study of High Temperature Solid Oxide Electrolysis Cell with Metal Foam." *Sustainability* 14:7064. https://doi.org/10.3390/su14127064.

Zheng, Y., Q. Li, T. Chen, W. Wu, C. Xu, and W. G. Wang. 2015. "Comparison of Performance and Degradation of Large-Scale Solid Oxide Electrolysis Cells in Stack with Different Composite air Electrodes." *International Journal of Hydrogen Energy* 40:2460–2472. https://doi.org/10.1016/j.ijhydene.2014.12.101.